HHS Public Access

Author manuscript

Neuroimage. Author manuscript; available in PMC 2019 May 15.

Published in final edited form as:

Neuroimage. 2018 May 15; 172: 64–84. doi:10.1016/j.neuroimage.2018.01.019.

Incorporating Spatial Constraint in Co-activation Pattern Analysis to Explore the Dynamics of Resting-State Networks: an Application to Parkinson's Disease

Xiaowei Zhuang[a,1], **Ryan R Walsh**[b,1], **Karthik Sreenivasan**[a], **Zhengshi Yang**[a], **Virendra Mishra**[a], and **Dietmar Cordes**[a,c,*]

[a]Cleveland Clinic Lou Ruvo Center for Brain Health, Las Vegas, NV 89106

[b]Department of Neurology, Barrow Neurological Institute, Phoenix, AZ 85013

[c]Department of Psychology and Neuroscience, University of Colorado Boulder, Boulder, CO 80309

Abstract

The dynamics of the brain's intrinsic networks have been recently studied using co-activation pattern (CAP) analysis. The CAP method relies on few model assumptions and CAP-based measurements provide quantitative information of network temporal dynamics. One limitation of existing CAP-related methods is that the computed CAPs share considerable spatial overlap that may or may not be functionally distinct relative to specific network dynamics. To more accurately describe network dynamics with spatially distinct CAPs, and to compare network dynamics between different populations, a novel data-driven CAP group analysis method is proposed in this study. In the proposed method, a dominant-CAP (d-CAP) set is synthesized across CAPs from multiple clustering runs for each group with the constraint of low spatial similarities among d-CAPs. Alternating d-CAPs with less overlapping spatial patterns can better capture overall network dynamics. The number of d-CAPs, the temporal fraction and spatial consistency of each d-CAP, and the subject-specific switching probability among all d-CAPs are then calculated for each group and used to compare network dynamics between groups.

The spatial dissimilarities among d-CAPs computed with the proposed method were first demonstrated using simulated data. High consistency between simulated ground-truth and computed d-CAPs was achieved, and detailed comparisons between the proposed method and existing CAP-based methods were conducted using simulated data. In an effort to physiologically validate the proposed technique and investigate network dynamics in a relevant brain network disorder, the proposed method was then applied to data from the Parkinson's Progression Markers Initiative (PPMI) database to compare the network dynamics in Parkinson's disease (PD) and normal control (NC) groups. Fewer d-CAPs, skewed distribution of temporal fractions of d-CAPs,

*Correspondence to: Dietmar Cordes, Ph.D., Cleveland Clinic Lou Ruvo Center for Brain Health, 888 W. Bonneville Ave, Las Vegas, NV, 89106, cordesd@ccf.org, Phone: 1-702-483-6022, Fax: 1-866-372-2720.

[1]The authors contributed equally to this study.

and reduced switching probabilities among final d-CAPs were found in most networks in the PD group, as compared to the NC group. Furthermore, an overall negative association between switching probability among d-CAPs and disease severity was observed in most networks in the PD group as well. These results expand upon previous findings from in vivo electrophysiological recording studies in PD. Importantly, this novel analysis also demonstrates that changes in network dynamics can be measured using resting-state fMRI data from subjects with early stage PD.

Keywords

co-activation pattern analysis; resting-state network temporal dynamics; d-CAP; switching probability; Parkinson's disease

1. Introduction

In the past two decades, brain functional connectivity has been widely studied using resting-state functional magnetic resonance imaging (fMRI). Functional connectivity is most commonly assessed using the Pearson correlation coefficient between fMRI signals from different regions in the brain (Biswal et al., 1995). Several functional connectivity studies have identified sets of spatial patterns that consist of temporally correlated brain regions (Biswal et al., 1995; De Luca et al., 2005; Greicius et al., 2003). These spatial patterns are called resting-state networks. Among the most commonly studied resting-state networks are the default mode network, sensorimotor network, visual network, auditory network and executive control network (Beckmann et al., 2005; Damoiseaux et al., 2006; Smith et al., 2009). Investigating resting-state networks has provided fundamental insight into basic neural function (Fox et al., 2005; Smith et al., 2009). Recent studies have shown, however, that the spatial patterns of resting-state networks may change periodically during the epoch of an fMRI scan (Preti et al., 2017). Dynamic functional connectivity analysis has been proposed to identify and investigate these changes in functional connectivity over time (Allen et al., 2014; Hutchison et al., 2013; Preti et al., 2017). Importantly, altered dynamic functional connectivity has recently been reported in neurological disorders such as schizophrenia (Damaraju et al., 2014; Yu et al., 2015), major depression disorder (Holtzheimer and Mayberg, 2011), autism (Price et al., 2014) and Alzheimer's disease (Jones et al., 2012), suggesting that such network changes have pathophysiologic relevance across brain diseases. Investigating dynamic functional connectivity in diseased populations can thus provide vital insight related to poorly understood dynamic brain function in these conditions, and lead to better understanding of disease phenotype, response to therapy, and progression.

Many methods have been proposed for dynamic functional connectivity analysis, such as the sliding-window method (Chang and Glover, 2010), temporal independent component analysis (ICA) (Smith et al., 2012), quasi-periodic pattern method (Majeed et al., 2011; Thompson et al., 2014), and co-activation pattern analysis (Liu and Duyn, 2013). The sliding-window method captures the dynamics of functional connectivity by gathering pairwise linear correlations among brain regions in subsequent temporal windows (Jones et al., 2012; Kucyi and Davis, 2014). Due to its relative simplicity, the sliding-window method

is the most widely applied technique in dynamic functional connectivity analysis. One technical challenge of this method, however, is the choice of the window size. Ideally, the window size should be small enough to capture any transients but also large enough to produce stable and statistically powerful results (Hutchison et al., 2013). Temporal ICA decomposes the entire fMRI time series into temporally independent components. Each component is then defined as a distinct temporal functional mode and used to represent the temporal dynamics of functional connectivity (Calhoun et al., 2001; Smith et al., 2012). Temporal ICA is, however, limited by the lack of sample points in conventional resting-state fMRI setting, where approximately 200 time points are typically collected in a 6–10 minute acquisition. The Quasi-periodic pattern method identifies a repeated spatiotemporal template within an fMRI scan (Majeed et al., 2011; Thompson et al., 2014). This template is a set of consecutive brain volumes represented throughout the entire scan. Dynamic functional connectivity is then represented by spatiotemporal patterns within this template. This method requires that the spatiotemporal pattern occurs several times during the course of data acquisition, implying that the quasi-periodic pattern method will only capture reproducible dynamic functional connectivity but will miss isolated (yet still potentially important) patterns of dynamic connectivity.

More recently, co-activation pattern (CAP) analysis has been proposed by Liu and Duyn (2013) to track variations of functional connectivity within each individual time frame. Instead of capturing dynamics of whole-brain functional connectivity, the CAP analysis focuses on the temporal dynamics of a specific resting-state network. The basis of CAP analysis is that relevant information of a given resting-state network is expressed by discrete time points where the fMRI signal is large (Chialvo, 2012; Tagliazucchi et al., 2011). Thus in CAP analysis, whole brain fMRI volumes at time points with large fMRI signals are temporally clustered using *k-means* into a predefined number of CAPs to reflect the dynamic behavior of a particular resting-state network.

One advantage of this method is that CAP analysis focuses on individual time frames and therefore does not require a large number of input time points as compared to the analysis methods mentioned above. Furthermore, the CAP method captures a more direct relationship between voxels as compared to the correlation-based sliding window method (Liu and Duyn, 2013). Importantly, the CAP analysis can be extended to whole brain analysis with the entire fMRI volume being input into temporal clustering (Liu et al., 2013). In addition to analysis of basic network dynamics in healthy controls, CAP analysis has also been used to investigate resting-state network dynamics related to cognition. Amico et al. (2014) found different CAPs associated with the default mode network across varying states of consciousness in healthy controls. Of particular importance, the CAP method can also be used to *quantify* brain dynamics relative to a behavior of interest. For example, measurements such as percentage of temporal occurrence of each CAP and the frequency of switches between all CAPs during an entire scan have been calculated in Chen et al. (2015). They reported a skewed distribution of CAP temporal occurrence and a higher switching frequency among different CAPs as evidence of reduced dynamics of the default mode network during task performance when compared to rest.

Despite these analytic advantages for the investigation of network dynamics, there is an important technical limitation of this method related to the dependence of CAP number on the choice of predefined numbers of clusters. Since any predefined number of CAPs can be computed using *k-means*, the functional distinction of each individual CAP cannot be guaranteed and some of the CAPs may share considerable spatial overlap. Furthermore, there is no current group analysis method to compare CAPs and study differences or similarities in brain dynamics between different populations.

In this study, we propose a novel CAP group analysis method that determines functionally distinct CAPs without a predefined temporal clustering number. In our proposed method, the final CAP set is synthesized across *k-means* results with multiple clustering numbers and with the important constraint of low spatial similarity between each final CAP. Furthermore, the proposed method also includes novel quantitative comparisons of network dynamics between different populations. In particular, subject-specific switching probability among the final CAPs is defined for this comparison. Using simulated data, we demonstrate that the proposed method accurately identifies functionally distinct CAPs for different groups.

A potential application of the proposed CAP group analysis is to enable development of imaging biomarkers that can characterize the temporal dynamics of resting-state brain networks in diseased populations. Parkinson's disease (PD) is a common neurodegenerative disorder with motor dysfunction as a major symptom, and with known brain network dysfunction associated with the disorder, including neurophysiological changes within the basal ganglia-thalamo-cortical circuits (Alexander, 1986; Brown et al., 2001; Holtbernd and Eidelberg, 2012; Litvak et al., 2011). Functional MRI techniques have provided further insights into corresponding functional connectivity changes in the PD population. Altered functional connectivity has been reported between the basal ganglia (mostly striatum) and the thalamus, midbrain, pons, cerebellum, mesolimbic pathway and the motor cortex using resting-state fMRI in different stages of PD (Baudrexel et al., 2011; Brittain et al., 2014; Esposito et al., 2013; Hacker et al., 2012; Helmich et al., 2012; Kwak et al., 2010; Luo et al., 2014; Palmer et al., 2010; Prodoehl et al., 2014; Sharman et al., 2013; Tessitore et al., 2012; Wu et al., 2012; Yu et al., 2015). Most recently, altered whole-brain dynamic functional connectivity has been reported in PD using the sliding-window method (Díez-Cirarda et al., 2017; Kim et al., 2017). Despite electrophysiologic data suggesting altered network dynamics associated with PD, however, network-focused temporal dynamic changes utilizing fMRI, have not yet been explored. In this study we explored the dynamics of resting-state networks in PD patients with the proposed CAP group analysis method. Previous intraoperative electrophysiological data have shown that the occurrence of motor symptoms in PD is associated with abnormally increased functional connectivity between the sub-thalamic and cortical regions, primarily in the α and β frequency bands (8–20 Hz) (Brittain et al., 2014; Brown, 2007; Chen et al., 2007; Eusebio et al., 2011; Oswal et al., 2013; Stein and Bar-Gad, 2013; Weiss et al., 2015). This altered synchronization within and between brain regions directly correlates with how long the nuclei from two regions (e.g. subthalamic nucleus and globus pallidus) remain functionally coupled (Cagnan et al., 2015; de Hemptinne et al., 2015; Escobar et al., 2017; Yanagisawa et al., 2012). Thus, due at least in part to the pathologically prolonged period of such aberrant synchronization, the overall dynamic range of network circuits appears to be limited in PD and importantly this

correlates with the degree of motor dysfunction observed in PD patients (Beck et al., 2016; Cagnan et al., 2015). Thus, we hypothesized that there would be reduced dynamics in sub-cortical and motor related resting-state networks in PD subjects compared to healthy subjects. We hypothesized that such reduced dynamics in PD subjects could be quantified by the novel proposed CAP-based measurements. Specifically, we hypothesized that the subject-specific CAP switching probability would be associated with motor symptom severity in each PD subject and therefore serve as a possible imaging biomarker to characterize pathologic temporal dynamics of resting-state networks in PD.

2. Methods

2.1 Group CAP analysis routine

2.1.1 Overview of previously published CAP methods—In the original CAP analysis proposed by Liu and Duyn (2013), a seed region is first selected and the fMRI signal is averaged within this region of interest (ROI). Subsequently, only time points with seed signal intensities larger than a chosen threshold are retained. Whole brain fMRI volumes at these specific time-points are then temporally clustered with a predefined cluster number k using *k-means*. CAPs are defined as the temporal-average spatial map of each cluster (Liu and Duyn, 2013). The occurrence percentage of each cluster is defined as the temporal fraction of the corresponding CAP. Spatial correlation is then computed between the average spatial map of each cluster (CAP) and the spatial map corresponding to each fMRI time frame that is a member of the cluster. Spatial consistency of each CAP is then defined as the average spatial correlation within the cluster (Liu et al., 2013; Liu and Duyn, 2013).

Chen et al. (2015) introduce the concept of an ‘overall dominant-CAP set’, which is a set of CAPs synthesized across results from *k-means* runs with multiple predefined cluster numbers k. An overall dominant CAP set represents key dynamic structures inherent in the network pattern and is computed in two steps. First, for each k of the *k-means* run, a dominant CAP (d-CAP) set is determined to select CAPs that make large contributions (as measured by the spatial similarities of selected CAPs and the overall time frame average) to the network pattern. The overall d-CAP set is then computed to be the most reproducible patterns among d-CAP sets from different cluster runs with different ks. Both the number of overall d-CAPs and the spatial correlation among each overall d-CAP are calculated to measure brain network dynamics (Chen et al., 2015). Furthermore, Chen et al. (2015) also calculate the switching frequency of CAPs. Since this measurement depends on the number of CAPs, an estimated cluster number is required. Chen et al. (2015) select the most representative cluster number $k = 2$ based on the silhouette score criteria. Temporal fraction and switching frequency of two CAPs are then calculated to specify brain network dynamics.

Our proposed novel CAP group analysis method is shown in Fig. 1. In short, the proposed method determines a dominant CAP (d-CAP) set for each subject group and computes four d-CAP related measurements to quantitatively compare network-related dynamics between groups. Specifically, the proposed method synthesizes CAPs across different clustering runs with the constraint of spatial dissimilarity among final d-CAPs incorporated, such that d-

CAP-based measurements more accurately represent network dynamics. Furthermore, the proposed method emphasizes the correspondence of the first few d-CAPs in the compared groups, therefore a more direct network comparison between different groups can be made. In the following sections, we explain each step of the proposed group CAP analysis routine in detail.

2.1.2 Determine dominant-CAP set for each group

Determine fMRI signals at network-associated time points: Conventional CAP analysis uses a single seed ROI to determine fMRI volumes that are associated with a specific resting-state network. Since multiple brain regions are involved in a given network, fMRI time frames associated with a particular network can be different based on different selected seed regions. To avoid this confound and obtain an overall network time signature, multiple seed ROIs are selected for a given resting-state network in the proposed method. Furthermore, seed ROIs are selected for each group separately to preserve group-related network changes. fMRI signals from multiple seed locations are then averaged to create one time course for each subject. Time points where averaged seed signal intensities pass a chosen threshold (such as top 20%) are defined as *network-associated* time points. Whole brain fMRI signals at network-associated time points are then determined from each subject in both groups and concatenated in time.

Determine CAP set: Temporal clustering is performed on concatenated time frames *from both groups* to guarantee the correspondence of CAPs from two groups. Time frames are clustered based on their spatial similarities, and clustering is done using *k-means* with multiple cluster numbers k (k = 1,2,3, …). Note that when k = 1, all network-associated time frames are clustered into one group. For each cluster number k, a group-specific CAP set is determined. Specifically, group-specific CAP sets $S_1^{k_i}$ and $S_2^{k_i}$ (the superscript k_i denotes the i^{th} cluster of a total of k clusters, i = 1,2, …, k, and the subscripts 1 or 2 represent group assignment) are computed by averaging spatial maps corresponding to time frames assigned to the cluster from group 1 and group 2, respectively.

Determine dominant-CAP set of each group: In the proposed method, we compute one d-CAP set for each group individually with every CAP from different *k-means* runs as equal candidates to avoid undue influence from any single *k-means* run on CAP determination. The final d-CAP set synthesizes the clustering results from multiple *k-means* runs and captures dynamic structures inherent in the network-associated time frames. In the following we explain how the d-CAP set is determined for group 1 and the same process is repeated for group 2.

First, for each cluster run k, the CAPs ($S_1^{k_i}$, i = 1,2, …, k) are re-ranked based on their temporal occurrences in descending order. The re-ordered CAPs from all cluster runs (k = 1,2,3,…) are combined to form the d-CAP candidate set, which is $\text{d-CAP}_{\text{candidate}} = \left\{ S_1^{1_1}, S_1^{2_1}, S_1^{2_2}, S_1^{3_1}, \ldots, S_1^{k_i} \middle| i = 1, 2, \ldots, k; k = 1, 2, 3 \ldots \right\}$. Since the average spatial

pattern of all network-associated time frames ($S_1^{1_1}$) reproduces the spatial profile of the corresponding resting-state network (Chialvo, 2012; Liu and Duyn, 2013), $S_1^{1_1}$ carries the major network spatial information and is initialized as the first element of the d-CAP set (d-CAP^1) for the group. Next, for every d-CAP candidate corresponding to the *k-means* run with $k = 2\,(S_1^{2_i}, i = 1, 2)$, we calculate the spatial similarity r_{jk_i} (i = 1,2; k = 2; j = 1, which is the number of current d-CAPs) between $S_1^{2_i}\,(i = 1, 2)$ and d-CAP^1:

$$r_{jk_i} = \text{corr}\,(\text{d-CAP}^j, S_1^{2_i}), \text{where } i = 1, 2; k = 2; \text{and } j = 1.$$

A threshold $thre_{jk_i}$ is also calculated for each d- CAP^1 and $S_1^{2_i}\,(i = 1, 2)$ pair. Let us first consider i = 1. The null hypothesis is that $S_1^{2_1}$ is spatially similar to the d-CAP^1 and can be represented by the d-CAP^1. To reject the null hypothesis, we generate the null distribution of r_{12_1} non-parametrically by permutation. We first convert the spatial map $S_1^{2_1}$ into a vector $S_{1_{vec}}^{2_1}$. Next, the vector $S_{1_{vec}}^{2_1}$ is randomly permuted and converted back to a spatial map $\tilde{S}_1^{2_1}$. The spatial map $\tilde{S}_1^{2_1}$ is then smoothed using an 8mm 3D Gaussian filter (the same smoothness as in $S_1^{2_1}$). Finally, we calculate the correlation between d-CAP^1 and smoothed $\tilde{S}_1^{2_1}$. This permutation process is repeated multiple times to create a stable null distribution of r_{12_1}. $Thre_{12_1}$ is then set to 5th percentile of the left tail of the null distribution (equivalent to 95th percentile of the right tail of the null distribution of one minus correlation value). If $r_{12_1} < thre_{12_1}$, and both r_{12_1} and the absolute difference between r_{12_1} and $thre_{12_1}$ are greater than 0.001, $S_1^{2_1}$ is added to the d-CAP set and the updated d-CAP set now has two elements d-CAP$^1 = S_1^{1_1}$ and d-CAP$^2 = S_1^{2_1}$. The latter criterion is included to avoid candidates with noisy spatial patterns being added to the d-CAP set. Subsequently, for the next d-CAP candidate $S_1^{2_2}$ we calculate spatial similarities (r_{j2_2}; j = 1, 2) between $S_1^{2_2}$ and all elements of the d-CAP set (d-CAP^1 and d-CAP^2). As detailed earlier, a set of thresholds $thre_{j2_2}$ (j = 1, 2) is also calculated. Importantly, only when $r_{j2_2}$is less than $thre_{j2_2}$ for both j = 1,2 is $S_1^{2_2}$ included in the d-CAP set. In this way, spatial dissimilarities among final d-CAPs are maintained. The above steps are repeated for all remaining d-CAP candidates $S_1^{k_i}$ (i = 1,2, …, k and k = 3, 4, ….) and a final d-CAP set is then determined for group 1. The same process is repeated for group 2. Figure 2 illustrates the process to compute the d-CAP set.

2.1.3 Measurements of CAP-based network dynamics—After the final d-CAP set is determined for each group, fMRI signals at network-associated time points are then assigned to different clusters based on their spatial similarities to final d-CAPs. Spatial correlations between each network-associated time frame and every d-CAP are calculated and used to specify the spatial similarity. Measurements of network dynamics are then calculated based on the new cluster assignment.

Number of d-CAPs: Since the entire process of computing the d-CAP set of each group is data-driven, the number of d-CAPs automatically represents network-associated dynamics in each group. Thus, fewer d-CAPs indicate a less dynamic network.

Temporal fraction: The temporal fraction (TF) is used to quantify how long a given network stays in one d-CAP during an entire scan, and is defined for each d-CAP as following: (similar to Liu and Duyn (2013)):

$$TF_j = \frac{\text{number of time frames assigned to dCAP}^j}{\text{number of network associated time frames}}, j = 1, 2, \ldots, \text{number of d-CAPs.}$$

Thus, a skewed distribution of temporal occurrences indicates that one group spends more time in one or more d-CAPs and demonstrates decreased network dynamics.

Spatial consistency: For each d-CAP cluster, the correlation between an individual network-associated time frame and the corresponding d-CAP map is also calculated and averaged to determine the spatial consistency. A more stable spatial consistency together with a higher temporal fraction represents a less dynamic resting-state network.

Switching probability: For each subject, we calculate the switching probability of d-CAPs associated with every resting-state network as a subject-specific measurement for network-associated dynamics. Network-associated time frames are reassigned to each d-CAP as mentioned above. For every subject, if two consecutively selected time frames belong to two different d-CAPs, a d-CAP switch is said to have occurred. The switching probability (SP) is then defined for that subject by

$$SP_s = \frac{\text{Number of dCAP switches}}{\text{Number of network associated time frames for subject s}}, s = 1, 2, \ldots, \text{number of subjects.}$$

A two sample t-test is then performed to test whether the switching probability is significantly different between two groups. A reduced switching probability reflects a less dynamic network.

2.2 Simulation

The simulation aimed both at examining whether the proposed CAP group analysis method could correctly determine the d-CAP set in different populations and at elucidating differences between the proposed method and traditional CAP analysis methods (Chen et al.,

2015; Liu and Duyn, 2013). To this end, two simulations were created from real fMRI time series (fMRI data acquisition detailed in section 2.3.1).

2.2.1 Simulation with two d-CAPs—In the first simulation, two groups of synthetic data were created from real fMRI time series. In each group, two spatially distinct d-CAPs were simulated to represent network temporal dynamics. Furthermore, the 1st d-CAP (d-CAP^1) was simulated to share common spatial patterns between two groups and the 2nd d-CAP (d-CAP^2) was simulated to contain different spatial patterns between two groups.

Simulate spatial patterns of d-CAPs: Spatial patterns of simulated d-CAPs were from real fMRI data. Time frames associated with the sensori-motor network in both groups were first selected and clustered into two clusters using *k-means* and CAPs were determined for each group (i.e. $S_1^{2_1}, S_1^{2_2}$ for group 1 and $S_2^{2_1}, S_2^{2_2}$ for group 2). Next, we calculated between-group spatial correlations for every axial slice in d-CAP^1 and d-CAP^2, and within-group spatial correlations for every axial slice between d-CAP^1 and d-CAP^2. The first slice which showed a high between-group spatial similarity (correlation value greater than 0.6) in d-CAP^1, a distinct spatial pattern (correlation value less than 0.4) in d-CAP^2 between two groups, and distinct spatial patterns between d-CAP^1 and d-CAP^2 in each group was identified as the *ground-truth slice* (*slice*$_t$). Spatial patterns of the ground-truth slice were then used as spatial patterns of d-CAP^1 (*slice*$_t$ of $S_1^{2_1}$ and $S_2^{2_1}$) and d-CAP^2 (*slice*$_t$ of $S_1^{2_2}$ and $S_2^{2_2}$) in the simulation (Fig. 3-1(A)). In this case, the spatial correlations between two groups were 0.95 and 0.14 for simulated d-CAP^1 and d-CAP^2, respectively. The spatial correlation between d-CAP^1 and d-CAP^2 was −0.57 for group 1 and −0.37 for group 2.

Simulate fMRI time series: Next, we generated fMRI time series associated with simulated d-CAPs for both groups. First, real fMRI time series of voxels within the ground-truth slice in group 1 were selected. Spatial correlations (r) between fMRI signals at every time point and the simulated d-CAP pair were calculated. fMRI time points at which the spatial pattern was highly correlated to either of the simulated d-CAPs ($r \geq 0.6$) were kept. In this way, we kept 414 time points with spatial patterns similar to the d-CAPs in group 1. These time points were further assigned to d-CAP^1 or d-CAP^2 clusters based on their spatial similarities with a particular d-CAP. Based on these criteria, 281 and 133 time points were assigned to d-CAP^1 and d-CAP^2 in group 1, respectively. Within each d-CAP cluster, the spatial covariance structure of the d-CAP was also calculated. The same procedure was repeated for group 2 with a total of 438 time points. Among these time points, 310 were assigned to d-CAP^1 and 128 were assigned to d-CAP^2.

The same number of time points associated with real-case d-CAP^1 was then simulated in each group. For group 1, we created 281 time points associated with d-CAP^1 and 133 time points associated with d-CAP^2. Noiseless spatial patterns of time points associated with d-CAP^1 and d-CAP^2 were generated by assigning spatial patterns of simulated d-CAP^1 and d-CAP^2 to the corresponding time points, respectively. Similarly, spatial patterns of d-CAP^1 and d-CAP^2 were assigned to the 310 and 128 time points associated with simulated d-CAP^1 and d-CAP^2 in group 2. Gaussian distributed noise with zero means and the same covariance

structure as in each real d-CAP cluster were then added to noiseless fMRI signals at corresponding time points in both groups. Finally, we generated fMRI signals that were associated with simulated d-CAPs and which contained the same noise structure as in real fMRI data.

2.2.2 Simulation with three d-CAPs—In this simulation, three d-CAPs were generated for each group to represent more complex network-dynamics. Specifically, in both groups, the 1st and 3rd d-CAPs (d-CAP^1 and d-CAP^3) were simulated to share spatial overlaps in group 1 and the 2nd d-CAP was simulated to be spatially distinct from d-CAP^1 and d-CAP^3 in both groups. More importantly, all three d-CAPs were simulated to have correspondences between two groups to better represent experimental observations.

Simulate d-CAPs: Spatial patterns of simulated d-CAPs were generated in the same way as in section 2.2.1. Time frames associated with the sensorimotor network in both groups were selected and clustered into three clusters using *k-means*. Spatial maps of CAPs were determined for each group separately. Next, we calculated the within-group spatial correlations of every axial slice between each d-CAP pair in group 1 and 2, respectively. The first slice which showed a spatial overlap between d-CAP^1 and d-CAP^3 in group 1 and a distinct spatial pattern of d-CAP^2 in both groups was identified as the ground-truth slice ($slice_t$). Spatial patterns of the ground-truth slice were then used as spatial patterns of d-CAP^1 ($slice_t$ of $S_1^{3_1}$ and $S_2^{3_1}$), d-CAP^2 ($slice_t$ of $S_1^{3_2}$ and $S_2^{3_2}$), and d-CAP^3 ($slice_t$ of $S_1^{3_3}$ and $S_2^{3_3}$) in this simulation (Fig. 4-1(A)). In this case, the spatial correlations between d-CAP^1 and d-CAP^3 were 0.25 and 0.13 for group 1 and group 2, respectively. The spatial correlation between d-CAP^1 and d-CAP^2 was −0.06 for group 1 and −0.02 for group 2, respectively.

Simulated fMRI time series: Real fMRI time series of voxels within the ground-truth slice were selected, and only time points at which the spatial pattern was similar to one of the simulated d-CAPs were kept. In this way, we kept 471 time points with spatial patterns similar to d-CAPs in group 1. These time points were further assigned to each d-CAP cluster based on their spatial similarities with the particular d-CAP. Based on these criteria, 177, 148 and 146 time points were assigned to d-CAP^1, d-CAP^2 and d-CAP^3 in group 1, respectively. Within each d-CAP cluster, the spatial covariance structure of the d-CAP was then calculated. The same procedure was repeated for group 2. A total of 445 time points were retained and among these time points, 192, 135 and 118 were assigned to d-CAP^1, d-CAP^2 and d-CAP^3 separately. The simulated time series is then generated the same way as described in section 2.2.1.

2.2.3 Analysis of simulated data—Simulated fMRI data generated in section 2.2.1 and 2.2.2 were considered as network-associated time frames and input into both the original CAP analysis (Chen et al., 2015; Liu and Duyn, 2013) and the proposed CAP group analysis.

Original CAP analysis: CAPs with selected k: CAPs were computed by following Liu and Duyn (2013). Specifically, the temporal clustering was performed using *k-means*. Distance measurement in *k-means* was $1 - cc$, where is the spatial correlation coefficient. The number of clusters (k) was determined by the silhouette score, which is a measurement of how well a member fits in a cluster (Chen et al., 2015; Rousseeuw, 1987). The CAPs with selected were then compared with the simulated ground truth.

Original CAP analysis: Overall dominant CAP set: The overall dominant CAP set for each group was computed as described in Chen et al. (2015). Briefly, temporal clustering was performed using *k-means* with cluster number $k = 2,3, \ldots,16$ on concatenated time series from both groups. For each *k-means* run, CAPs were computed for each group separately and selected CAPs that made large contributions to the network pattern were determined to be the dominant CAP set for that k. The overall dominant CAP set was then selected as the most reproducible patterns among dominant CAP sets from different cluster runs with different ks and compared with the simulated ground truth.

The proposed CAP group analysis: Temporal clustering was performed using *k-means* with cluster number $k = 2,3, \ldots,20$ on concatenated time series from both groups. For each cluster run, *k-means* was repeated multiple times to account for the instability of a single trial run. d-CAP sets for each group were then synthesized across results from multiple cluster runs. The number of d-CAPs was determined for each group and compared with the ground truth. The spatial correlation between each d-CAP and ground-truth d-CAP map pair was also calculated and used to evaluate the performance of the proposed method.

2.3 Exploring resting-state network dynamics in Parkinson's disease with the group CAP analysis method

2.3.1 Subjects and Experiments

Subjects: The data used in this study were obtained from the publicly available anonymized Parkinson's Progression Markers Initiative (PPMI) database [Marek et al., 2011]. For up-to-date information, please visit http://www.ppmi-info.org. The PPMI is a landmark, large-scale, comprehensive, observational, international, multi-center study that recruits de novo (early-untreated) PD patients and age-matched healthy normal subjects (NCs) to identify PD progression biomarkers.

We included 18 NCs (14 Male (M); age: 64.25±9.50 years (mean ± SD)) and 20 newly diagnosed, early-stage, and never medicated PD subjects (11 M; age: 58.03±11.54 years; disease duration: 1.01±1.07 years) from the PPMI database in our analysis. Both advancing disease and medication in PD subjects produce confounding effects on the functional integration and organization of intrinsic brain networks (Luo et al., 2014), therefore we only included PD subjects who were at an early stage of disease and never-medicated. PD subjects were assessed for symptom severity around the MRI scanning time using the motor portion (Part III) of the Unified Parkinson's Disease Rating Scale (UPDRS). Each PD subject was further rated on a subscale for tremor defined by both tremor at rest and action or postural tremor of the hands (Mure et al., 2011; Vo et al., 2017). Symptoms for PD were considered to be *tremor-dominant* if the summed limb UPDRS-III tremor score was ≥ 4 with

at least one limb scoring ≥ 2 (Isaias et al., 2010; Mure et al., 2011; Vo et al., 2017). Tremor-dominant PD subjects may have different pathophysiology compared to other PD subjects (Helmich et al., 2012), and therefore to maintain a relatively homogenous group PD subjects kept in our analysis were non-tremor dominant (UPDRS-III motor score: 15.05±7.43; tremor score: 1.25±1.04). This criterion also avoids the potential confound of tremor on image acquisition as well. A Chi-square test was performed to check statistical significance for gender difference between two groups and Wilcoxon rank sum test was performed to check for differences of age and year of education. Information about subject demographics, UPDRS motor and tremor scores are listed in Table 1.

MRI acquisition: All subjects underwent resting-state fMRI scans on 3T Siemens scanners. The resting-state fMRI involved an 8 minutes and 24 seconds acquisition with 210 time frames, TR = 2400ms, TE = 25ms, FOV = 22.4 cm, flip angle = 80deg, resolution = 3.3 × 3.3 × 3.3 mm^3, 40 axial slices. In addition, a T1-weighted structural image was also acquired for each subject with TR = 2300ms, TE = 2.98ms, flip angle = 9deg, and voxel size = 1 × 1 × 1 mm^3.

fMRI preprocessing: The first 5 time frames (12sec) were removed to allow the MR signal to achieve T1 equilibrium. Time frames were slice-timing corrected and realigned to the mean echo-planar image in SPM12 (http://www.fil.ion.ucl.ac.uk/spm/), further co-registered to the subject T1 space, and then normalized to the standard MNI-152 2mm-template using ANTs software (http://stnava.github.io/ANTs/). Six head motion parameters, signals extracted from subject white matter and cerebrospinal fluid (3-mm cubes centered at MNI (26,−12, 35) and (19,−33, 18)), were regressed out from each dataset. fMRI data were further spatially smoothed using an 8mm 3D-Gaussian filter. All voxel time courses were band pass filtered (0.008Hz<f<0.1Hz) to emphasize low-frequency correlations in the resting-state, and variance normalized.

2.3.2 CAP group analysis—Preprocessed resting-state fMRI data from both groups were concatenated in time and input to a spatial independent component analysis (ICA) to compute major accepted resting-state networks. In our analysis, voxels within the skull-stripped MNI-152 2mm template and having non-zero signal intensities in all subjects were included in the brain mask. The ICA decomposition was carried out with the fast-ICA algorithm [Hyvärinen et al., 2001] using an in-house MATLAB program. The number of components was set to 20. Seven resting-state networks were chosen that were consistent with previous reports (Beckmann et al., 2005; Smith et al., 2009). In particular, we chose the default mode network (DMN), left and right frontal-parietal network (FPN), sub-cortical network, sensorimotor network (SMN), executive control network (ECN), visual network (VN, including both primary and lateral visual networks) and auditory network (AUD). Another ICA component including the middle temporal gyrus and the superior temporal gyrus was also found with our data and defined as the medial temporal network (MTN). Since dysfunction in PD subjects is known to involve sub-cortical and cortical functional loops (Hacker et al., 2012), we focused our CAP group analysis on relevant ICA-based cortical networks (DMN, FPN, SMN, ECN and MTN) and two seed-based sub-cortical

networks (sub-thalamic seeded network (STh) and striatum seeded network (STR)). Spatial maps of these seven resting-state networks are shown in Fig. 5.

Seeds for each resting-state network were selected for two groups individually. For ICA networks, group specific maps for PD and NC were computed using dual regression (Beckmann et al., 2009). Peak location of each cluster in the network spatial map was then determined. 3mm cubes centered at each peak location were then selected as seed ROIs for the resting-state network. Seeds for sub-cortical networks (STh and STR) were obtained from an anatomical probabilistic atlas of the basal ganglia (ATAG-template; (Keuken et al., 2013)). Specifically, seeds for the STh network involved two 3mm cubes centered at left and right sub-thalamus, and seeds for the STR network involved four 3mm cubes centered at left and right putamen and caudate. Table 2 lists seed coordinates for the seven networks chosen in this study.

A static group network comparison was first carried out using seed-based correlation maps from every subject for the DMN, FPN, SMN, ECN, MTN, STh, and STR networks separately. fMRI signals from multiple seed locations of one resting-state network (Table 2) were averaged to create a single seed time course of the network. For every subject, a seed-based network map was computed by calculating the Pearson correlation between the time course of each brain voxel and the reference seed time course. A two-sample t-test was performed to detect between-group differences in each network. Significant differences were detected using “Threshold-Free Cluster Enhancement” as implemented in FSL (Smith and Nichols, 2009), with $p<0.05$ family-wise error corrected and spatially masked with the thresholded group average correlation map.

Next, time frames with seed signal intensity in the top 20% (41 time frames) of each subject were selected as network-associated time frames. The average spatial map of network-associated time frames was compared with the seed-based network pattern to verify whether selected time frames were truly associated with the network. The percentage threshold (20%) was determined by following the method of Liu and Dyun (2013). We varied the percentage threshold from 0% to 100% in steps of 10% and plotted the spatial correlation value between the average spatial map of selected time frames and the seed-based correlation map as a function of percentage thresholds. We found that when the top 20% of time frames were selected, the curve reached a plateau and the spatial correlation surpassed 0.95 validating this method.

Network associated time frames from both groups were then concatenated in time and decomposed into different CAPs based on their spatial similarities using *k-means*. The number of clusters (k) in *k-means* was varied from 2 to 20. For each k, we repeated the clustering process 120 times to account for the instability of single-trial *k-means* results and selected the best clustering result with the smallest within-cluster sum of point-to-centroid distances. After clustering, a d-CAP candidate set was determined for each group and a final d-CAP set was then computed from the candidate set as described in section 2.1.2. Specifically, in adding each d-CAP candidate into the final d-CAP set, we repeated the voxel-wise permutations multiple times and calculated the cumulative null distribution of the spatial similarity for every 10 permutations. The 5^{th} percentile of each cumulative null

distribution was then computed and plotted against the number of permutations involved. Once the change of the 5th percentile value between the current and previous cumulative null distribution was less than 5%, we stopped the permutation step. The 5th percentile of the current cumulative null distribution was then set as the threshold (*thre*). Finally, the spatial pattern of each d-CAP was then converted to a z-score map.

For each resting-state network, the number of d-CAPs was determined to enable the description of temporal dynamics in each group. Temporal fraction and spatial consistency were then calculated for each d-CAP and used to compare the network dynamics between PD and NC groups. For networks with the same number of d-CAPs in both groups, the temporal fraction for the 1st d-CAP was also calculated for each subject. Two sample t-test was performed to test between-group differences of the occurrence of the 1st d-CAP in these networks. Furthermore, a null distribution of the spatial consistency for each d-CAP was also generated to test the reliability of the final d-CAPs. To generate the null distribution of spatial consistency, network-associated time points were first randomly assigned to each d-CAP cluster with the same temporal fraction as the corresponding d-CAP. The spatial profile of the corresponding d-CAP was then updated with the average spatial map within each cluster. The average correlation between an individual time frame and the updated d-CAP map was finally calculated for every cluster and considered as one entry of the null distribution. The above process was repeated multiple times until a stable null distribution was generated. The real spatial consistency of each d-CAP was then compared with the 95th percentile of the null distribution to test the reliability of each final d-CAP cluster at the significance level of $p=0.05$.

For each resting-state network, the switching probabilities among all final d-CAPs were then calculated for each subject. A two sample t-test was performed on switching probabilities with age, gender, years of education, handedness, and scanner sites as covariates between two groups to compare the network temporal dynamics in PD and NC. Significance level was established at $p<0.05$, family-wise corrected for seven comparisons (seven resting-state networks, Bonferroni corrected). T-statistic, corrected p-value, and effect size for every comparison were reported.

We further investigated the association between network dynamic changes and symptom severity in PD subjects. For each resting-state network, a multiple linear regression analysis was performed between the switching probability (*SP*) and the UPDRS-III motor score with age, gender, year of education, handedness, and scanner sites as covariates (of no interest) in the PD group:

$$\boldsymbol{SP} = \boldsymbol{\beta}_0 + \boldsymbol{X}_{motor}\beta_{motor} + \boldsymbol{X}_{covariates}\boldsymbol{\beta}_{covariates} + \boldsymbol{\varepsilon},$$

where $\boldsymbol{X}_{motor}$ was subject UPDRS-III motor score, $\boldsymbol{X}_{covariates}$ was a metric including subject age, gender, year of education, handedness, or scanner site, and ε was the residual error term. Statistical significance level for β_{motor} was established at $p<0.05$ (Bonferroni corrected for seven comparisons). Effect size for β_{motor} of each network was reported.

3. Results

3.1 Simulation

Simulation with two d-CAPs: The spatial patterns of simulated ground truth are shown in Fig. 3-1(A). The results computed from the previous method in Liu and Duyn (2013) are shown in Fig. 3-2. $k = 2$ gives the highest silhouette score in the *k-means* clustering (Fig. 3-2(A)) and the corresponding two CAPs (Liu and Duyn 2013) are shown in Fig. 3-2(B). The spatial similarity between the simulated ground truth (Fig. 3-1(A)) and the CAPs with selected k (Fig. 3-1(B)) is shown in Fig. 3-2(C) by the spatial correlation matrices. The overall dominant CAPs (Chen et al., 2015) are shown in Fig. 3-3(A) and the spatial similarity to the ground truth (Fig. 3-1(A)) is reflected by the correlation matrix in Fig 3-3(B). The final d-CAP set of each group computed by the proposed CAP method is shown in Fig. 3-1(B). The similarity between the simulated ground-truth (Fig. 3-1(A)) and d-CAPs (Fig. 3-1(B)) is shown in Fig. 3-1(C).

As shown in Fig. 3, all three CAP methods were able to compute sets of CAPs, overall dominant CAPs or d-CAPs to represent temporal dynamics. Both k CAPs selected by the silhouette score and d-CAPs computed from the proposed method were able to precisely recover the simulated ground truth in each group. The average spatial correlation values were 0.91± 0.09 (mean± standard deviation) between d-CAPs and simulated ground truth (Fig. 3-1(C)) and 0.85±0.03 between k CAPs and the ground truth (Fig 3-2 (C)). The overall dominant CAP set (Fig. 3-2(B)) also captured the temporal variation, as four overall dominant CAPs were computed for group 1 and three were computed for group 2. Since there was no spatial constraint in computing the overall dominant CAP set, the 2nd and 3rd overall dominant CAPs in group 1 showed a high spatial similarity and both of them represent the d-CAP^1 in the ground truth. Similarly, both the 1st and 4th overall dominant CAPs in group 1 recovered the d-CAP^2 in the simulated ground truth. In addition, d-CAPs calculated from the proposed method incorporated constraints on spatial correlation values between the final d-CAP pairs, and therefore distinct spatial maps were precisely recovered (Fig 3-1(C)). Furthermore, and as expected, with the proposed method excellent correspondence ($r > 0.9$) was observed between the spatial patterns of 1st d-CAPs from two groups.

Simulation with three d-CAPs: As shown in Fig. 4-2 (A), $k = 2$ gives the highest silhouette score in the *k-means* clustering and the corresponding two CAPs (Liu and Duyn 2013) are shown in Fig. 4-2(B). The spatial similarity between the simulated ground truth (Fig. 4-1(A)) and the CAPs with selected k is reflected by the correlation matrices and shown in Fig. 4-2(C). The overall dominant CAPs (Chen et al., 2015) are shown in Fig. 4-3(A) and the spatial similarity to the ground truth (Fig. 4-1(A)) is shown in Fig 4-3(B). The final d-CAP set of each group computed by the proposed CAP method is shown in Fig. 4-1(B). The similarity between the simulated ground-truth (Fig. 4-1(A)) and d-CAPs (Fig. 4-1(B)) is shown in Fig. 4-1(C).

As shown in Fig. 4-2, for simulation with more than two d-CAPs, CAPs selected by silhouette criteria combined the 1st and 2nd simulated d-CAPs and therefore missed an

important contribution to the temporal dynamics (Fig. 4-2). The overall dominant CAP set (Chen et al., 2015) in this simulation recovered three d-CAPs in group 1, which demonstrates the ability of this method to accurately identify dynamic states. However, since spatial constraint is still not incorporated in computing overall dominant CAP sets, the 3rd and 4th overall dominant CAPs represent the same simulated d-CAP3 in group 2 (Fig. 4-3). Using our proposed method, high consistency (r>0.8) is achieved between d-CAPs and the simulated ground truth.

Overall, the simulation results demonstrate that the proposed group CAP analysis can accurately determine the d-CAP set in different populations, which is not the case for the previously suggested methods.

3.2 Comparison of network dynamics between PD and NC groups

3.2.1 Demographics—Table 1 lists the demographics of both PD and NC subjects used in this study. Age (p=0.10), gender (p=0.13) and years of education (p=0.78) were not significantly different between the two groups. Motor performance, as measured by UPDRS III motor score, was significantly different between the two groups (p<0.001, Table. 1). Furthermore, PD subjects with summed limb UPDRS III scores was ≤ 4 and with at least one limb scoring ≤ 2 were included in this study. As for NC subjects, the summed limb UPDRS III scores were all 0, except for one subject (with a score of 1). For motion calculation, rotational displacements were converted to translational displacements by projection to a surface of a 50mm radius sphere and root-mean-square (RMS) head motion was computed for every subject (Power et al., 2014). All subjects had less than one voxel size (0.51mm on average) RMS head motion and RMS head motion was not significantly different between the PD and NC groups (p = 0.38, Table. 1).

3.2.2 Static network comparison—Significant between-group differences in static network spatial patterns were only observed in the MTN and ECN. Increased left medial temporal connections were observed in the MTN, and stronger middle frontal connections were observed in the MTN in the NC group.

3.2.3 Null distribution of spatial similarity between two maps—On average, 100 times voxel-wise permutations were repeated to obtain a stable null distribution in determining every d-CAP in each network separately. Two examples with either a positive or a negative spatial correlation between the existing d-CAP and the current d-CAP candidate are shown in Fig. 6. Fig. 6-1(A) and Fig. 6-2(A) list spatial maps of the existing d-CAP (top part) and the current d-CAP candidate (bottom part), with a spatial correlation value of 0.09 between maps in Fig. 6-1(A) and −0.21 in Fig. 6-2(A). The threshold (*thre*) to determine whether two maps are spatially similar is plotted in Fig. 6-1(B) and Fig. 6-2(B) as a function of number of permutations being performed. As can be seen from Fig. 6-1 (B) and Fig. 6-2(B), the change of the threshold when including 100 permutations is less than 5%. Fig. 6-1(C) and Fig. 6-2(C) further show the histogram of null correlation values of 1000 permutations and the 5th percentile of the left tail (*thre*, red dashed line). The change of *thre* computed by 100 and 1000 permutations is less than 1% in both cases.

3.2.4 Dominant CAP (d-CAP) sets of the PD and NC groups—Using the proposed CAP group analysis method, we computed a set of d-CAPs for every resting-state network in the PD and NC groups separately. The total number of d-CAPs associated with each resting-state network is listed in Table 3. Spatial patterns of the blood oxygen level-dependent (BOLD) signal for the final d-CAP sets are shown in Fig. 7-1. Spatial maps of every d-CAP are converted to effect size (Cohen's d) maps, thresholded at $d \geq 0.8$ (large effect), and shown in Fig. 7-2. Between-group differences in Cohen's d maps for each d-CAP are summarized in Table 4. Spatial similarities between d-CAPs are represented by correlation matrices and shown in each box in Fig. 7-3. The between group d-CAP spatial similarities are shown in the bottom left plot in each box, and within group similarities for the NC and PD groups are shown in the top left and bottom right in each box respectively.

Distinct spatial patterns were observed between d-CAPs from the same group in all seven resting-state networks (Fig. 7-1). The average correlation values between within-group d-CAPs were 0.14 ± 0.14 (mean ± standard deviation) for the PD group and 0.12 ± 0.15 for the NC group.

As listed in Table 3-1, the same number of d-CAPs were computed for the DMN, FPN, SMN, and STR networks in both study groups. Good correspondence was observed in d-CAPs associated with these four networks between the PD and NC groups (Fig. 7-1), with an average spatial correlation value between the corresponding d-CAPs of 0.84±0.08. Closer examination of voxels with a large effect size in each network revealed differences in co-activation patterns between d-CAPs of the two groups (red arrows in Fig. 7-2 and summarized in Table 4). Increased co-activation (indicated by large effect size) between sub-cortical and motor areas (2^{nd} d-CAP of SMN and 3^{rd} d-CAP of STR), as well as between the striatum and frontal areas (1^{st} d-CAP of the STR) were observed in the NC group (Fig. 7-2 and Table 4(A)). On the other hand, larger activity was observed in the superior temporal lobe, middle frontal regions (2^{nd} d-CAP of the DMN), and the inferior parietal lobe (2^{nd} d-CAP of the FPN) in the PD group (Fig. 7-2 and Table 4(B)).

For the ECN, MTN, and STh networks, an additional d-CAP was determined for the NC group (Table 3), indicating that these networks were more dynamic in NC subjects when compared to PD subjects. The additional d-CAP (4^{th} d-CAP) of the ECN in the NC group showed a distinct pattern of co-activations in the anterior and posterior cingulate cortex and precuneus regions. The extra d-CAPs of the MTN, ECN, and STh networks showed sub-cortical connections with the medial temporal area and the anterior cingulate cortex (Fig. 7-2 and Table 4). In the remaining d-CAPs for these three networks, we observed a high spatial similarity of corresponding d-CAPs between NC and PD groups with an average correlation value of 0.83±0.08 (Fig. 7-3). Despite the high spatial similarity, different patterns of co-activation were observed in the corresponding d-CAPs in both groups. Distinct co-activation pattern of sub-cortical regions and motor areas were observed in the 2^{nd} d-CAP of the STh network in the NC group. In addition, an increase of sub-cortical connections with the medial temporal lobe and the frontal lobe is also shown in the 2^{nd} d-CAP of the MTN and ECN in the NC group.

3.2.5 Temporal fraction and spatial consistency of each d-CAP—Table 5(A) lists the temporal fraction of the d-CAPs associated with each resting-state network. The average temporal fraction of the 1st d-CAP associated with all seven resting-state networks was 61.17% ±10.29% for the NC group and 68.00% ± 8.65% for the PD group. Furthermore, for networks with the same number of d-CAPs in the two groups (DMN, FPN, SMN, and STR), Table 5(B) lists the mean and standard deviation of the temporal fraction of the 1st d-CAPs in each group and the result from a group comparison. While no significant differences ($p<0.05$, Bonferroni corrected) were found for any network, higher temporal fractions of the 1st d-CAP of the DMN, SMN, and STR networks were observed in the PD group with a moderate effect size (Cohen's d=0.58, 0.57 and 0.49 respectively). In contrast, a higher temporal fraction in the 1st d-CAP was also observed in the FPN in the NC group with very small effect size (d = 0.09).

The spatial consistency of each d-CAP associated with the seven resting-state networks is listed in Table 6. The 95th percentile of the null distribution of each consistency is also listed in brackets in Table 6. The average spatial consistency of all d-CAPs was 0.34 ± 0.02 in the NC group and 0.30 ± 0.02 in the PD group, which is similar to the value reported by Liu and Duyn (2013). In addition, the spatial consistency of every d-CAP was greater than the 95th percentile of the null distribution, indicating that the spatial consistency of all d-CAPs was significant ($p<0.05$, non-parametric).

3.2.6 Switching probability of each resting-state network—The switching probability was computed for every subject in the PD and NC groups. Box plots of d-CAP switching probability associated with the seven resting-state networks are shown in Fig. 8. Significant ($p<0.05$, Bonferroni corrected) decreases in switching probabilities were observed in the ECN ($p=0.05$, effect size d =1.04), MTN ($p=1.9\times10^{-4}$, d=1.77) and STh ($p=2.7\times10^{-5}$, d=2.01) networks in the PD group when compared to NC group (Fig. 8 and Table 7). There were no significant differences found in the other networks. The DMN, SMN, and STR networks did exhibit expected decreasing trends in switching probability in PD compared to controls, however, with an effect size (d) of 0.79 for the DMN, 0.62 for the SMN, and 0.89 for the STR (Table 6). Furthermore, a relatively higher median of switching probability in the FPN was observed in the PD group (Fig. 8) but with a very small effect size (d=0.05, Table 7). Overall, reduced switching probabilities in the PD group compared to the NC group reflects overall reduced dynamics in PD networks as hypothesized.

3.2.7 Correlation of PD symptoms with network temporal dynamics—Fig. 9 shows the relationship between network dynamic changes (switching probability) and clinical symptoms (UPDRS-III motor score) in the PD group. The fitted line (solid red) and the 95% confidence interval of the estimation (dashed green) are shown in Fig. 9. A significant negative relationship was observed between the switching probability of the SMN d-CAPs and the UPDRS-III motor score of each PD subject ($p = 0.04$, d = 0.88, Table 8). There were no statistically significant relationships between the switching probability and the UPDRS-III motor score of the other six networks. A negative trend between the switching probability and the UPDRS-III motor score was observed, however, in the ECN (d = 0.25, Table 8), MTN (d = 0.22, Table 8), STh (d = 0.12, Table 8), and STR (d = 0.18,

Table 8). On the other hand, a positive trend was observed for the DMN (d = 0.15) and FPN (d = 0.22).

4. Discussion

In this study, we proposed a novel group CAP analysis method to analyze temporal dynamics of specific resting-state networks for different populations. We introduced a new method to synthesize CAPs across different clustering runs with spatial distinction among final d-CAPs. Four d-CAP based measurements were calculated to compare network dynamics between different populations. Using simulation, we demonstrated that our method was able to determine spatially distinct d-CAPs *without* a predefined clustering number. We further used the proposed method to perform a novel investigation of network dynamics in PD and NC groups without a priori assumption. We observed altered network co-activated patterns and temporal dynamics in the PD group that reflect and expand upon prior understanding of PD network pathophysiology, including in relation to symptom severity.

4.1 Methodological perspectives

4.1.1. Major innovations

Spatial constraints in determining d-CAPs: In CAP-based analysis, two concepts have been proposed to represent the variation of network spatial patterns over time: the CAP set in Liu and Duyn (2013) and the overall dominant CAP set in Chen et al. (2015). Since spatial independence is not a requirement in either method, however, the CAPs or overall d-CAPs can share considerable spatial overlap and may or may not have functionally distinct significance. Using simulation, we have demonstrated that two overall dominant CAPs that share small spatial variations may possibly be the result of one overall dominant CAP being split into two simply due to noise in the clustering step (See Fig. 3-3 and Fig. 4-3). As a result, the switching between these two CAPs (or overall d-CAPs) might not be real and could confound understanding of the overall network dynamics.

One major innovation of the proposed method is that the constraint of low spatial similarities among final d-CAPs is incorporated in synthesizing over clustering results with different s. In our analysis the spatial similarity is reflected by the spatial correlation value, where a higher spatial correlation indicates a larger overlap in activated areas within the network spatial pattern. Furthermore, if there are multiple spatially distinct CAPs accounting for temporal variations of network-associated time frames, *k-means* clustering will identify these patterns and the proposed method will treat them equally as d-CAP candidates. Even though the final d-CAPs in our analysis cannot be said to be fully spatially independent, they are spatially statistically different at the significance level of $p<0.05$. Furthermore, alternating d-CAPs with less overlapping spatial patterns can make important contributions to overall network dynamics. This key property of the proposed method is demonstrated using simulated data. We simulated d-CAPs with spatial correlation values varied from −0.57 to 0.25 and our method was able to recover them with high accuracy (Fig. 3-1 and Fig. 4-1). Furthermore, the correlation matrices for each d-CAP pair utilizing the real fMRI data show low correlation values (r) along the off-diagonal line in Fig. 7-3. This observation

suggests that the final d-CAPs are not spatially overlapping, which demonstrates that our method computes spatially distinct d-CAPs.

Group analysis: In the current CAP analysis method the group comparison is done by comparing the CAP (or overall d-CAP) sets (a) computed for different groups separately (Chen et al., 2015) or (b) computed by using a benchmark CAP set determined from healthy subjects as a reference (Amico et al., 2014). As shown by simulation (Fig. 3-3 and 4-3), the first method does not maintain the correspondence of CAPs (or overall d-CAPs) from different populations and therefore does not enable direct comparisons. The reference CAP set in the second method is not data-driven and therefore may not accurately represent network dynamics in diseased populations where such dynamics are difficult to predict. To make a fair comparison between different groups while retaining group-specific network dynamics, we perform the temporal clustering on concatenated network-associated time frames from both groups *together*. Group-specific CAP sets ($S_1^{k_i}$ and $S_2^{k_i}$) are then determined separately and treated as d-CAP candidates for each group (2^{nd} and 3^{rd} boxes in Fig. 1). In this case, final d-CAP sets for both groups are computed from the same clustering results and therefore the variation of clustering will not affect the between-group comparisons of d-CAP based measurements. As shown in both simulation (Fig. 3-1 and Fig. 4-1) and real fMRI data (Fig. 7), excellent correspondence is observed in most d-CAPs between the two groups in our analysis.

4.1.2. Information embedded in d-CAP based measurements—The CAP analysis focuses on the temporal dynamics of each resting-state network, and therefore provides a new dimension in characterizing network behaviors (Liu and Duyn, 2013). Chen et al. (2015) introduced four CAP-based quantifiable metrics to reveal brain dynamics, including: the *quantity* of overall-dominant CAPs, the *spatial consistency* across different CAPs, the *temporal fractions* of CAPs, and the *frequency of state alternation* in CAPs.

In the proposed method, the d-CAP set reflects the embedded network-associated dynamics. Since the process in determining d-CAPs in our novel analysis is purely data-driven and spatial similarities among d-CAPs are constrained with non-parametrical statistics, the number of d-CAPs directly and more faithfully describes and accommodates network temporal diversity (Table 3 and Fig. 7). Furthermore, the d-CAP set serves as the basis of all the quantifiable measurements calculated subsequently.

The spatial consistency across different CAPs is calculated in Chen et al. (2015) to quantify the uniformity of brain dynamics. In our method, however, due to the incorporated constraint of low spatial similarities among final d-CAPs the spatial consistency across different CAPs is not computed. Rather, spatial consistency of each d-CAP provides information about the *stability* of d-CAPs. As listed in Table 5, spatial consistency values of every d-CAP surpass the 95^{th} percentile of the null distribution and therefore confirm the reliability of d-CAPs calculated from the proposed method.

In Chen et al. (2015), both the temporal fractions and frequency of alternating CAP states depend heavily on the predefined CAP number. An additional criterion using silhouette

score is applied to determine the most representative cluster number. As shown by the simulation, CAPs selected by silhouette score may incorrectly combine several distinct CAPs into a single CAP due to clustering with a fixed cluster number k (Fig. 4-2). In our analysis, alternating network spatial patterns are tracked at each individual time frame level. The temporal fraction is then calculated for each final d-CAP which provides information regarding how long the network stays in each d-CAP. As listed in Table 4, the temporal fraction of the 1st d-CAP is the largest for every network suggesting that the 1st d-CAP is the most common state for all networks. The 1st d-CAP is the spatial average of all network-associated time frames, and therefore represents the overall network spatial profile (Liu and Duyn, 2013; Tagliazucchi et al., 2011). The frequency of alternating states is defined as switching probability in our analysis and used to quantify the frequency of d-CAP alternations throughout the entire fMRI scan.

Each of the above four measurements (*number* of d-CAPs, *temporal fraction*, *spatial consistency* of each d-CAP, and the *switching probability* among all d-CAPs) provides a different perspective in quantifying network-associated dynamics and can be used for group comparisons. It is important to note, however, that these four metrics are not independent. In our analysis, all four measurements are based on the final d-CAP set. For example, a smaller number of d-CAPs will result in a longer time spent in one or all d-CAPs in one population and therefore automatically lead to a smaller switching probability among network-associated time frames. At the same time, a smaller number of d-CAPs already demonstrates dynamic changes from one state to another. In this regard, the number of d-CAPs, temporal fraction of each d-CAP, and the switching probability among all d-CAPs share common information in group comparisons and should be properly interpreted. Spatial consistency, in addition to the other three measures, provides *complementary* information about the stability of each d-CAP.

4.1.3 Parameter selection

Threshold to determine network-associated time frames: The CAP analysis is based on the concept that the resting-state network is driven primarily by activities at a few discrete events (Liu and Duyn, 2013; Tagliazucchi et al., 2011). These discrete time points share a common feature that the signal intensity at the core regions of the resting-state network is relatively large. We define these as network-associated time frames.

The threshold to determine network-associated time frames remains unclear. Liu and Duyn (2013) compared the average of time frames whose signal at the seed region surpassed a predefined threshold to the seed-based correlation map computed using all time frames. They found that similarity between the two maps increases rapidly when lowering the threshold and approaches a plateau after including 15% of all time frames. We have repeated the same method and found that when the top 20% time frames were included with our dataset, the similarity between two maps reaches a plateau. The variation in the threshold is mainly due to the smaller sample size used in our study (38), compared to Liu and Duyn (2013) (247). In this case, more time frames per subject are needed to account for subject variability. In addition, this threshold is set to be the top 30% in Chen et al. (2015) where even fewer subjects were included (21). Furthermore, in our analysis, time series at each

voxel are converted to z-score and therefore follow a standard normal distribution. When the top 20% time frames are selected, the lowest signal intensity is approximately z = 0.7 and at about 70% of the standard normal distribution.

Features used in k-means clustering: In the proposed method, features used in the *k-means* clustering are signal intensities at each voxel and a skull-stripped brain mask is applied in our analysis. There are two reasons to do a voxel-wise CAP analysis instead of ROI-wise CAP analysis as in Chen et al. (2015). First, all network-associated time frames are related to a specific resting-state network. The proposed method is mainly used to analyze the variation of each network-spatial pattern and, therefore, the change among CAPs can be voxel-wise structures instead of large ROIs. Second, averaging signals within each ROI may affect the constraint in determining final d-CAPs.

4.2 Altered resting-state network dynamics in the PD group

In our analysis, examining the spatial patterns of d-CAPs for each group provides information regarding alternating networks whereas comparing the d-CAP based measurements between two groups provides characterization of altered network temporal dynamics.

4.2.1 Functional disturbances in the spatial domain of the PD group—Static network comparisons between the PD and NC groups have shown enhanced functional connectivity in the left medial temporal lobe in the MTN and the medial frontal area in the ECN in the NC group. These stronger connections were also observed in the 3rd and 4th d-CAPs in the NC groups (Fig. 7-2). All other observed differences in d-CAPs were not observed with conventional methods due to the temporal stationarity assumption.

Previous studies using resting-state fMRI have uncovered inconsistent changes in functional connectivity of PD subjects at various disease stages (Badea et al., 2017; Prodoehl et al., 2014; Tahmasian et al., 2017, 2015). Specifically, in the early stage of the disease PD subjects exhibit reduced functional connectivity in cortico-striatal loops before they start medication (Esposito et al., 2013; Luo et al., 2014). As the disease progresses and medication starts having an effect, increased functional connectivity between the sub-thalamic nuclei and the motor cortex has been reported (Baudrexel et al., 2011; Kwak et al., 2010). When the disease reaches its advanced stages, the striatal connections with the thalamus, midbrain, pons and cerebellum, and the DMN connection are again found to be decreasing (Hacker et al., 2012; Tessitore et al., 2012). In the two subcortical networks focused on in our analysis, weaker connections are observed between the sub-thalamus and the motor area (2nd d-CAP of the STh), between the striatum and the motor area (3rd d-CAP of the STR), and between the striatum and the frontal area (1st d-CAP of the STR) in the PD group, which is consistent with the above reports. Furthermore, in cortical networks, stronger subcortical connections with the frontal area, the medial temporal lobe, and the motor area are revealed in the 2nd d-CAP of the ECN, MTN, and SMN in the NC group separately, which further confirms the finding of reduced sub-cortical and cortical connections in PD subjects (Esposito et al., 2013; Luo et al., 2014). Overall, functional differences between the sub-cortical area (thalamus and striatum) and the cortical area

(frontal lobe, medial temporal lobe, and motor area) among PD and NC subjects are reflected in our d-CAP spatial patterns.

4.2.2 Altered dynamic functional connectivity in the PD group—The dynamics of basal ganglia-cortical circuits in PD subjects have been widely studied and reported using electrophysiological data, but correlations of these findings in imaging-based data are unclear. Specifically, un-medicated PD subjects exhibit aberrant coherent activity patterns and excessive synchronization of neuronal activities in the basal ganglia-cortical loop (Brown, 2007; Brown and Williams, 2005; Chen et al., 2007; Eusebio et al., 2011; Fries, 2005; Oswal et al., 2013; Stein and Bar-Gad, 2013). Exaggerated oscillations in the beta frequency band (~20Hz) are found to be correlated with the increased frequency and duration of locked phase alignments between the subthalamic nucleus and the globus pallidus (Brittain et al., 2014; Cagnan et al., 2015; Escobar et al., 2017; Weiss et al., 2015; Yanagisawa et al., 2012). Thus, basal-ganglia cortical circuits shift from a more dynamic phase-alignment to a prolonged locked phase-synchronization in PD subjects, which will in turn affect the neuronal circuits' dynamics (Cagnan et al., 2015; Weiss et al., 2015). Furthermore, the phase of this beta-oscillation in PD subjects is found to be excessively coupled with the amplitude of the broad band (50–200 Hz) activity in the primary motor cortex at rest (de Hemptinne et al., 2015). Importantly, the activity of the broad band is known to be linearly correlated with the BOLD signal measured by fMRI data (Canolty et al., 2006; Mukamel, 2005). Thus, we hypothesized that dynamics of neuronal circuits affected by the excessive phase synchronization in PD should also be reflected in reduced dynamics of resting-state networks in fMRI BOLD analysis.

Based on the above, we explored network dynamics in PD using resting-state fMRI BOLD data. We observed less dynamic sub-cortical (STh) and cortical networks (MTN and ECN) in the PD group, as reflected both by the decreased number of d-CAPs and the significantly reduced d-CAP switching probabilities (Table 3, Fig. 8) when compared to the NC group. These results corroborate and expand upon electrophysiologic findings of the shifted basal-ganglia cortical circuits in PD subjects (Cagnan et al., 2015; de Hemptinne et al., 2015; Weiss et al., 2015; Yanagisawa et al., 2012), and represent a novel investigation of network dynamics in PD using fMRI. In addition, the same number of d-CAPs was obtained in both groups for the DMN, FPN, SMN, and STR and a higher contribution of the 1st d-CAP was observed in the DMN, SMN, and STR (Table 5) in the PD group. Higher fractions of the first one or few d-CAPs indicates a skewed distribution of the temporal fraction, which in turn suggests less dynamic networks (Chen et al., 2015) as hypothesized. Reduced switching probabilities were also observed for these three networks with moderate effect size in the PD group (Table 7), which further demonstrates the limited dynamic range of brain networks in PD (de Hemptinne et al., 2015; Yanagisawa et al., 2012). In contrast, a higher temporal fraction of the 1st d-CAP and an increasing trend of the switching probability were observed for the FPN in the PD group. As shown in Fig. 7-2, both d-CAPs of the FPN in PD exhibit higher activities in the bilateral inferior parietal lobe. The functional increase in this area has previously been reported by a meta-analysis on 28 PD fMRI studies (Tahmasian et al., 2017). Tahmasian et al. (2017) conclude that the deficiency in the basal ganglia cortical loop at early PD stage is countered by the increased connectivity in other brain regions, which is

explained by a presumed compensatory mechanism. The same compensation process may also explain the altered dynamics of the FPN in our results, but since only small effect sizes were observed for the between group comparisons on temporal fraction (d=0.09) and switching probability (d=0.05) of the FPN, further investigations are required before any conclusions can be drawn in this regard.

Previous correlative evidence from electrophysiological data has suggested that excessive synchronization in the basal ganglia is associated with impairment of movement in PD (Brown and Williams, 2005; Chen et al., 2007; Kühn et al., 2009), and that the increased frequency and duration of locked phase-alignment is also correlated with the deteriorated motor function in PD subjects (Beck et al., 2016; Cagnan et al., 2015). We also observed a significant negative association ($p<0.001$) between the switching probability in the SMN and the UPDRS-III motor score in the PD group (3^{rd} subplot in Fig. 9 and Table 8), indicating that reduced network dynamics are associated with severity of PD clinical motor symptoms. Similarly negative trends between network dynamics and PD clinical symptoms are also observed in the FPN, ECN, MTN, STh, and STR. The SMN connects the major motor areas, sub-cortical areas, and cerebellum and therefore could be more sensitive to PD progression and thus reflected in our data with these early stage patients.

As shown in Fig. 9, significant reductions in switching probability in the ECN, MTN and STh networks are found in the PD group while decreasing associations with the UPDRS-III motor score are only evident at the trend level in these three networks. The significantly reduced switching probabilities of these networks demonstrate overall changes in dynamic network engagements from the normal state to the diseased state that were observed using the proposed method despite making no a priori assumptions. As for the SMN, even though the between-group difference in the switching probability is not statistically significant ($p=0.09$, uncorrected), the effect size of this comparison is moderate (Cohen's $d=0.65$, see Table. 6). Inclusion of more subjects would thus likely reach statistical significance in this case. The negative association of the SMN with the motor score likely indicates that the switching probability of the SMN is correlated with the decrease in motor performance in the PD group, perhaps as a result of impaired motor planning as well as execution. In addition, we also observed an increasing trend of switching probability as a function of UPDRS-III motor score in the PD group in the FPN and DMN although small effect size and larger variation limits interpretation.

Overall, we found altered, mostly reduced, network temporal dynamics in the PD group when compared to the NC group which corroborates and expands upon previous electrophysiological studies. Furthermore, to our knowledge this is the first imaging study to demonstrate such aberrant network-focused dynamics in PD, and demonstrates that such reduced network dynamics can be studied using resting-state fMRI data in PD. This proof of principle will be important in resting-state fMRI studies that are underway to improve diagnosis, understand response to treatment, and predict symptom development in PD, and may provide the foundation for an urgently-needed imaging-based biomarker for this disease (Walsh, 2016).

4.3 Limitations and future studies

In the proposed CAP group analysis, the temporal clustering on concatenated time frames is performed by *k-means* clustering with the spatial correlation as a similarity measure. This clustering method only captures pair-wise linear relationships between two time frames. The spatial similarity between different time frames in fMRI data may not be linear, however. In such a case, clustering methods that consider non-linear relationships between different observations, such as the *kernel k-means* method, could be applied to replace *k-means* clustering in determining CAPs. Substituting *k-means*-related methods with hierarchical clustering could also improve the clustering accuracy and efficiency.

In addition, in the proposed method group comparisons are done with the d-CAP based measurements. Direct comparisons between d-CAPs cannot be performed primarily because the d-CAP sets from the proposed analysis represent group-specific network dynamics. The correspondence of all d-CAPs (except d-CAP^1) between groups cannot be maintained. In this case, the between group comparisons cannot be performed directly using a specific d-CAP other than d-CAP^1.

As discussed above, the interdependence between the number of d-CAPs, the temporal fraction of each d-CAP, and the switching probability among all d-CAPs is inherently embedded in the proposed method. All three measurements are based on the d-CAP set in each group. In this case, results of the between group network dynamics comparisons using temporal fractions or switching probabilities should be properly interpreted. Furthermore, a possible means to obviate this interdependence is to compare temporal fractions or switching probabilities between two groups only when the two groups share the same number of d-CAPs.

5. Conclusions

In this study, we have proposed a novel group CAP analysis method to investigate temporal dynamics of specific resting-state networks. Our data-driven method computes less spatially overlapping d-CAPs for each group. Four d-CAP based measurements have been introduced to compare network dynamics between different populations. Using the proposed method, we have compared the dynamics of seven major resting-state networks between NC and PD groups. We have found reduced numbers of d-CAPs, skewed distribution of temporal fractions of d-CAPs, and reduced switching probabilities among final d-CAPs of most networks in the PD group, which represent novel imaging-based findings in this field. Furthermore, we have shown that switching probability is negatively correlated with the UPDRS-III motor score in PD subjects suggesting that aberrant network dynamics are related to disease symptomatology. Our analysis demonstrates that network dynamics can be studied using resting-state fMRI data.

Acknowledgments

The research was supported by the National Institute of Health (grant number 1R01EB014284 and P20GM109025).

Data used in the preparation of this article were obtained from the Parkinson's Progression Markers Initiative (PPMI) database (www.ppmi-info.org/data). For up-to-date information on the study, visit www.ppmi-info.org.

PPMI, a public-private partnership, is funded by the Michael J. Fox Foundation for Parkinson's Research. Other funding partners include a consortium of industry players, non-profit organizations and private individuals: AbbVie, Avid Radiopharmaceuticals, Biogen Idec, Bristol-Meyers Squibb, Covance, GE Healthcare, Genentech, GlaxoSmithKline, Eli Lilly and Company, Lundbeck, Merck, Meso Scale Discovery, Pfizer Inc., Piramal Imaging, Roche CNS group, Servier, UCB and Golub Capital.

References

Alexander G. Parallel Organization of Functionally Segregated Circuits Linking Basal Ganglia and Cortex. Annu Rev Neurosci. 1986; 9:357–381. https://doi.org/10.1146/annurev.neuro.9.1.357. [PubMed: 3085570]

Allen EA, Damaraju E, Plis SM, Erhardt EB, Eichele T, Calhoun VD. Tracking whole-brain connectivity dynamics in the resting state. Cereb Cortex. 2014; 24:663–676. https://doi.org/10.1093/cercor/bhs352. [PubMed: 23146964]

Amico E, Gomez F, Di Perri C, Vanhaudenhuyse A, Lesenfants D, Boveroux P, Bonhomme V, Brichant JF, Marinazzo D, Laureys S. Posterior cingulate cortex-related co-activation patterns: A resting state fMRI study in propofol-induced loss of consciousness. PLoS One. 2014; 9:e100012. https://doi.org/10.1371/journal.pone.0100012. [PubMed: 24979748]

Badea L, Onu M, Wu T, Roceanu A, Bajenaru O. Exploring the reproducibility of functional connectivity alterations in Parkinson's disease. PLoS One. 2017; 12:e0188196. https://doi.org/10.1371/journal.pone.0188196. [PubMed: 29182621]

Baudrexel S, Witte T, Seifried C, von Wegner F, Beissner F, Klein JC, Steinmetz H, Deichmann R, Roeper J, Hilker R. Resting state fMRI reveals increased subthalamic nucleus-motor cortex connectivity in Parkinson's disease. Neuroimage. 2011; 55:1728–1738. https://doi.org/10.1016/j.neuroimage.2011.01.017. [PubMed: 21255661]

Beck MH, Haumesser JK, Kühn J, Altschüler J, Kühn AA, van Riesen C. Short- and long-term dopamine depletion causes enhanced beta oscillations in the cortico-basal ganglia loop of parkinsonian rats. Exp Neurol. 2016; 286:124–136. https://doi.org/10.1016/j.expneurol.2016.10.005. [PubMed: 27743915]

Beckmann C, Mackay C, Filippini N, Smith S. Group comparison of resting-state FMRI data using multi-subject ICA and dual regression. Neuroimage. 2009; 47:S148. https://doi.org/10.1016/S1053-8119(09)71511-3.

Beckmann CF, DeLuca M, Devlin JT, Smith SM. Investigations into resting-state connectivity using independent component analysis. Philos Trans R Soc B Biol Sci. 2005; 360:1001–1013. https://doi.org/10.1098/rstb.2005.1634.

Biswal B, Zerrin Yetkin F, Haughton VM, Hyde JS. Functional connectivity in the motor cortex of resting human brain using echo planar mri. Magn Reson Med. 1995; 34:537–541. https://doi.org/10.1002/mrm.1910340409. [PubMed: 8524021]

Brittain JS, Sharott A, Brown P. The highs and lows of beta activity in cortico-basal ganglia loops. Eur J Neurosci. 2014; 39:1951–1959. https://doi.org/10.1111/ejn.12574. [PubMed: 24890470]

Brown P. Abnormal oscillatory synchronisation in the motor system leads to impaired movement. Curr Opin Neurobiol. 2007; 17:656–664. https://doi.org/10.1016/j.conb.2007.12.001. [PubMed: 18221864]

Brown P, Oliviero A, Mazzone P, Insola A, Tonali P, Di Lazzaro V. Dopamine dependency of oscillations between subthalamic nucleus and pallidum in Parkinson's disease. J Neurosci. 2001; 21:1033–1038. [pii]. [PubMed: 11157088]

Brown P, Williams D. Basal ganglia local field potential activity: character and functional significance in the human. Clin Neurophysiol. 2005; 116:2510–2519. https://doi.org/10.1016/j.clinph.2005.05.009. [PubMed: 16029963]

Cagnan H, Duff EP, Brown P. The relative phases of basal ganglia activities dynamically shape effective connectivity in Parkinson's disease. Brain. 2015; 138:1667–1678. https://doi.org/10.1093/brain/awv093. [PubMed: 25888552]

Calhoun VD, Adali T, Pearlson GD, Pekar JJ. Spatial and temporal independent component analysis of functional MRI data containing a pair of task-related waveforms. Hum Brain Mapp. 2001; 13:43–53. https://doi.org/10.1002/hbm.1024. [PubMed: 11284046]

Canolty RT, Edwards E, Dalal SS, Soltani M, Nagarajan SS, Kirsch HE, Berger MS, Barbaro NM, Knight RT. High Gamma Power Is Phase-Locked to Theta Oscillations in Human Neocortex. Science (80-). 2006; 313:1626–1628. https://doi.org/10.1126/science.1128115.

Chang C, Glover GH. NeuroImage Time – frequency dynamics of resting-state brain connectivity measured with fMRI. Neuroimage. 2010; 50:81–98. https://doi.org/10.1016/j.neuroimage.2009.12.011. [PubMed: 20006716]

Chen CCC, Litvak V, Gilbertson T, Kühn A, Kuhn A, Lu CS, Lee ST, Tsai CH, Tisch S, Limousin P, Hariz M, Brown P. Excessive synchronization of basal ganglia neurons at 20 Hz slows movement in Parkinson's disease. Exp Neurol. 2007; 205:214–221. https://doi.org/10.1016/j.expneurol.2007.01.027. [PubMed: 17335810]

Chen JE, Chang C, Greicius MD, Glover GH. Introducing co-activation pattern metrics to quantify spontaneous brain network dynamics. Neuroimage. 2015; 111:476–488. https://doi.org/10.1016/j.neuroimage.2015.01.057. [PubMed: 25662866]

Chialvo DR. Criticality in large-scale brain fMRI dynamics unveiled by a novel point process analysis. Front Physiol. 2012; 3:1–12. https://doi.org/10.3389/fphys.2012.00015. [PubMed: 22275902]

Damaraju E, Allen EA, Belger A, Ford JM, McEwen S, Mathalon DH, Mueller BA, Pearlson GD, Potkin SG, Preda A, Turner JA, Vaidya JG, Van Erp TG, Calhoun VD. Dynamic functional connectivity analysis reveals transient states of dysconnectivity in schizophrenia. NeuroImage Clin. 2014; 5:298–308. https://doi.org/10.1016/j.nicl.2014.07.003. [PubMed: 25161896]

Damoiseaux JS, Rombouts SARB, Barkhof F, Scheltens P, Stam CJ, Smith SM, Beckmann CF. Consistent resting-state networks across healthy subjects. Proc Natl Acad Sci. 2006; 103:13848–13853. https://doi.org/10.1073/pnas.0601417103. [PubMed: 16945915]

de Hemptinne C, Swann NC, Ostrem JL, Ryapolova-Webb ES, San Luciano M, Galifianakis NB, Starr PA. Therapeutic deep brain stimulation reduces cortical phase-amplitude coupling in Parkinson's disease. Nat Neurosci. 2015; 18:779–786. https://doi.org/10.1038/nn.3997. [PubMed: 25867121]

De Luca, M., Beckmann, CF., De Stefano, N., Matthews, PM., Smith, SM. fMRI resting state networks define distinct modes of long-distance interactions in the human brain Oxford Centre for Functional Magnetic Resonance Imaging of the Brain, UK. Neuroimage. 2005. https://doi.org/10.1016/j.neuroimage.2005.08.035

Escobar, D., Johnson, LA., Nebeck, SD., Zhang, J., Johnson, MD., Baker, KB., Molnar, GF., Vitek, JL. Parkinsonism and Vigilance: Alteration in neural oscillatory activity and phase-amplitude coupling in the basal ganglia and motor cortex; J Neurophysiol. 2017. p. 118jn.00388.2017. https://doi.org/10.1152/jn.00388.2017

Esposito F, Tessitore A, Giordano A, De Micco R, Paccone A, Conforti R, Pignataro G, Annunziato L, Tedeschi G. Rhythm-specific modulation of the sensorimotor network in drug-naïve patients with Parkinson's disease by levodopa. Brain. 2013; 136:710–725. https://doi.org/10.1093/brain/awt007. [PubMed: 23423673]

Eusebio A, Thevathasan W, Doyle Gaynor L, Pogosyan A, Bye E, Foltynie T, Zrinzo L, Ashkan K, Aziz T, Brown P. Deep brain stimulation can suppress pathological synchronisation in parkinsonian patients. J Neurol Neurosurg Psychiatry. 2011; 82:569–573. https://doi.org/10.1136/jnnp.2010.217489. [PubMed: 20935326]

Fox MD, Snyder AZ, Vincent JL, Corbetta M, Van Essen DC, Raichle ME. From The Cover: The human brain is intrinsically organized into dynamic, anticorrelated functional networks. Proc Natl Acad Sci. 2005; 102:9673–9678. https://doi.org/10.1073/pnas.0504136102. [PubMed: 15976020]

Fries P. A mechanism for cognitive dynamics: Neuronal communication through neuronal coherence. Trends Cogn Sci. 2005; 9:474–480. https://doi.org/10.1016/j.tics.2005.08.011. [PubMed: 16150631]

Greicius MD, Krasnow B, Reiss AL, Menon V. Functional connectivity in the resting brain: A network analysis of the default mode hypothesis. Proc Natl Acad Sci. 2003; 100:253–258. https://doi.org/10.1073/pnas.0135058100. [PubMed: 12506194]

Hacker CD, Perlmutter JS, Criswell SR, Ances BM, Snyder AZ. Resting state functional connectivity of the striatum in Parkinson's disease. Brain. 2012; 135:3699–3711. https://doi.org/10.1093/brain/aws281. [PubMed: 23195207]

Helmich RC, Hallett M, Deuschl G, Toni I, Bloem BR. Cerebral causes and consequences of parkinsonian resting tremor: A tale of two circuits? Brain. 2012; 135:3206–3226. https://doi.org/10.1093/brain/aws023. [PubMed: 22382359]

Holtbernd F, Eidelberg D. Functional brain networks in movement disorders. Curr Opin Neurol. 2012; 25:392–401. https://doi.org/10.1097/WCO.0b013e328355aa94. [PubMed: 22710361]

Holtzheimer PE, Mayberg HS. Stuck in a rut: Rethinking depression and its treatment. Trends Neurosci. 2011; 34:1–9. https://doi.org/10.1016/j.tins.2010.10.004. [PubMed: 21067824]

Hutchison RM, Womelsdorf T, Allen EA, Bandettini PA, Calhoun VD, Corbetta M, Della Penna S, Duyn JH, Glover GH, Gonzalez-Castillo J, Handwerker DA, Keilholz S, Kiviniemi V, Leopold DA, de Pasquale F, Sporns O, Walter M, Chang C. Dynamic functional connectivity: Promise, issues, and interpretations. Neuroimage. 2013; 80:360–378. https://doi.org/10.1016/j.neuroimage.2013.05.079. [PubMed: 23707587]

Isaias IU, Marotta G, Hirano S, Canesi M, Benti R, Righini A, Tang C, Cilia R, Pezzoli G, Eidelberg D, Antonini A. Imaging essential tremor. Mov Disord. 2010; 25:679–686. https://doi.org/10.1002/mds.22870. [PubMed: 20437537]

Jones, DT., Vemuri, P., Murphy, MC., Gunter, JL., Senjem, ML., Machulda, MM., Przybelski, SA., Gregg, BE., Kantarci, K., Knopman, DS., Boeve, BF., Petersen, RC., CRJ. Non-Stationarity in the "' Resting Brain's "' Modular Architecture; PLoS One. 2012. p. 7https://doi.org/10.1371/journal.pone.0039731

Keuken MC, Bazin PL, Schafer A, Neumann J, Turner R, Forstmann BU. Ultra-High 7T MRI of Structural Age-Related Changes of the Subthalamic Nucleus. J Neurosci. 2013; 33:4896–4900. https://doi.org/10.1523/JNEUROSCI.3241-12.2013. [PubMed: 23486960]

Kucyi A, Davis KD. NeuroImage Dynamic functional connectivity of the default mode network tracks daydreaming ☆. Neuroimage. 2014; 100:471–480. https://doi.org/10.1016/j.neuroimage.2014.06.044. [PubMed: 24973603]

Kühn AA, Tsui A, Aziz T, Ray N, Brücke C. Pathological synchronisation in the subthalamic nucleus of patients with Parkinson's disease …. Exp Neurol. 2009; 215:380–387. https://doi.org/10.1016/j.expneurol.2008.11.008. DOI: 10.1016/j.expneurol.2008.11.008 [PubMed: 19070616]

Kwak, Y., Peltier, S., Bohnen, NI., Müller, MLTM., Dayalu, P., Seidler, RD. Altered Resting State Cortico-Striatal Connectivity in Mild to Moderate Stage Parkinson's Disease; Front Syst Neurosci. 2010. p. 4https://doi.org/10.3389/fnsys.2010.00143

Litvak V, Jha A, Eusebio A, Oostenveld R, Foltynie T, Limousin P, Zrinzo L, Hariz MI, Friston K, Brown P. Resting oscillatory cortico-subthalamic connectivity in patients with Parkinson's disease. Brain. 2011; 134:359–374. https://doi.org/10.1093/brain/awq332. [PubMed: 21147836]

Liu, X., Chang, C., Duyn, JH. Decomposition of spontaneous brain activity into distinct fMRI co-activation patterns; Front Syst Neurosci. 2013. p. 7https://doi.org/10.3389/fnsys.2013.00101

Liu X, Duyn JH. Time-varying functional network information extracted from brief instances of spontaneous brain activity. Proc Natl Acad Sci. 2013; 110:4392–4397. https://doi.org/10.1073/pnas.1216856110. [PubMed: 23440216]

Luo C, Song W, Chen Q, Zheng Z, Chen K, Cao B, Yang J, Li J, Huang X, Gong Q, Shang H. Neurobiology of Aging Reduced functional connectivity in early-stage drug-naive Parkinson's disease: a resting-state fMRI study. Neurobiol Aging. 2014; 35:431–441. https://doi.org/10.1016/j.neurobiolaging.2013.08.018. [PubMed: 24074808]

Majeed W, Magnuson M, Hasenkamp W, Schwarb H, Schumacher EH, Barsalou L, Keilholz SD. Spatiotemporal dynamics of low frequency BOLD fluctuations in rats and humans. Neuroimage. 2011; 54:1140–1150. [pii]. [PubMed: 20728554]

Mukamel R. Coupling Between Neuronal Firing, Field Potentials, and fMRI in Human Auditory Cortex. Science (80-). 2005; 309:951–954. https://doi.org/10.1126/science.1110913.

Mure H, Hirano S, Tang CC, Isaias IU, Antonini A, Ma Y, Dhawan V, Eidelberg D. Parkinson's disease tremor-related metabolic network: Characterization, progression, and treatment effects. Neuroimage. 2011; 54:1244–1253. https://doi.org/10.1016/j.neuroimage.2010.09.028. [PubMed: 20851193]

Oswal A, Brown P, Litvak V. Synchronized neural oscillations and the pathophysiology of Parkinson's disease. Curr Opin Neurol. 2013; 26:662–670. https://doi.org/10.1097/WCO.0000000000000034. [PubMed: 24150222]

Palmer SJ, Li J, Wang ZJ, McKeown MJ. Joint amplitude and connectivity compensatory mechanisms in Parkinson's disease. Neuroscience. 2010; 166:1110–1118. https://doi.org/10.1016/j.neuroscience.2010.01.012. [PubMed: 20074617]

Power JD, Mitra A, Laumann TO, Snyder AZ, Schlaggar BL, Petersen SE. Methods to detect, characterize, and remove motion artifact in resting state fMRI. Neuroimage. 2014; 84:320–341. https://doi.org/10.1016/j.neuroimage.2013.08.048. [PubMed: 23994314]

Preti MG, Bolton TAW, Van De Ville D. The dynamic functional connectome: State-of-the-art and perspectives. Neuroimage. 2017; 160:41–54. https://doi.org/10.1016/j.neuroimage.2016.12.061. [PubMed: 28034766]

Price, T., Wee, C-Y., Gao, W., Shen, D. Multiple-Network Classification of Childhood Autism Using Functional Connectivity Dynamics. International Conference on Medical Image Computing and Computer-Assisted Intervention; 2014. p. 177-184.https://doi.org/10.1007/978-3-319-10443-0_23

Prodoehl J, Burciu RG, Vaillancourt DE. Resting state functional magnetic resonance imaging in Parkinson's disease. Curr Neurol Neurosci Rep. 2014; 14:448. https://doi.org/10.1007/s11910-014-0448-6. [PubMed: 24744021]

Rousseeuw PJ. Silhouettes: A graphical aid to the interpretation and validation of cluster analysis. J Comput Appl Math. 1987; 20:53–65. https://doi.org/10.1016/0377-0427(87)90125-7.

Sharman M, Valabregue R, Perlbarg V, Marrakchi-Kacem L, Vidailhet M, Benali H, Brice A, Lehéricy S. Parkinson's disease patients show reduced cortical-subcortical sensorimotor connectivity. Mov Disord. 2013; 28:447–454. https://doi.org/10.1002/mds.25255. [PubMed: 23144002]

Smith SM, Fox PT, Miller KL, Glahn DC, Fox PM, Mackay CE, Filippini N, Watkins KE, Toro R, Laird AR, Beckmann CF. Correspondence of the brain's functional architecture during activation and rest. Proc Natl Acad Sci. 2009; 106:13040–13045. https://doi.org/10.1073/pnas.0905267106. [PubMed: 19620724]

Smith SM, Miller KL, Moeller S, Xu J, Auerbach EJ, Woolrich MW, Beckmann CF, Jenkinson M, Andersson J, Glasser MF, Van Essen DC, Feinberg DA, Yacoub ES, Ugurbil K. Temporally-independent functional modes of spontaneous brain activity. Proc Natl Acad Sci. 2012; 109:3131–3136. https://doi.org/10.1073/pnas.1121329109. [PubMed: 22323591]

Smith SM, Nichols TE. Threshold-free cluster enhancement: Addressing problems of smoothing, threshold dependence and localisation in cluster inference. Neuroimage. 2009; 44:83–98. https://doi.org/10.1016/j.neuroimage.2008.03.061. [PubMed: 18501637]

Stein E, Bar-Gad I. Beta oscillations in the cortico-basal ganglia loop during parkinsonism. Exp Neurol. 2013; 245:52–59. https://doi.org/10.1016/j.expneurol.2012.07.023. [PubMed: 22921537]

Tagliazucchi E, Balenzuela P, Fraiman D, Montoya P, Chialvo DR. Spontaneous BOLD event triggered averages for estimating functional connectivity at resting state. Neurosci Lett. 2011; 488:158–163. https://doi.org/10.1016/j.neulet.2010.11.020. [PubMed: 21078369]

Tahmasian M, Bettray LM, van Eimeren T, Drzezga A, Timmermann L, Eickhoff CR, Eickhoff SB, Eggers C. A systematic review on the applications of resting-state fMRI in Parkinson's disease: Does dopamine replacement therapy play a role? Cortex. 2015; 73:80–105. https://doi.org/10.1016/j.cortex.2015.08.005. [PubMed: 26386442]

Tahmasian M, Eickhoff SB, Giehl K, Schwartz F, Herz DM, Drzezga A, Van Eimeren T, Laird AR, Fox PT. ScienceDirect Resting-state functional reorganization in Parkinson's disease: An activation likelihood estimation meta-analysis. Cortex. 2017; 92:119–138. https://doi.org/10.1016/j.cortex.2017.03.016. [PubMed: 28467917]

Tessitore A, Esposito F, Vitale C, Santangelo G, Amboni M, Russo A, Corbo D, Cirillo G, Barone P, Tedeschi G. Default-mode network connectivity in cognitively unimpaired patients with Parkinson disease. Neurology. 2012; 79:2226–2232. https://doi.org/10.1212/WNL.0b013e31827689d6. [PubMed: 23100395]

Thompson GJ, Pan WJ, Magnuson ME, Jaeger D, Keilholz SD. Quasi-periodic patterns (QPP): Large-scale dynamics in resting state fMRI that correlate with local infraslow electrical activity.

Neuroimage. 2014; 84:1018–1031. https://doi.org/10.1016/j.neuroimage.2013.09.029. [PubMed: 24071524]

Vo A, Sako W, Fujita K, Peng S, Mattis PJ, Skidmore FM, Ma Y, Uluğ AM, Eidelberg D. Parkinson's disease-related network topographies characterized with resting state functional MRI. Hum Brain Mapp. 2017; 38:617–630. https://doi.org/10.1002/hbm.23260. [PubMed: 27207613]

Walsh, RR. Parkinson's Disease: Current and Future Therapeutics and Clinical Trials - Google Books. In: Gálvez-Jiménez, N.Fernandez, HH.Espay, A., Fox, SE., editors. Parkinson's Disease: Current & Future Therapeutics & Clinical Trials. Cambridge University Press; Cambridge: 2016.

Weiss, D., Klotz, R., Govindan, RB., Scholten, M., Naros, G., Ramos-Murguialday, A., Bunjes, F., Meisner, C., Plewnia, C., Krüger, R., Gharabaghi, A. Subthalamic stimulation modulates cortical motor network activity and synchronization in Parkinson's disease; Brain. 2015. p. 1-15.https://doi.org/10.1093/brain/awu380

Wu T, Wang J, Wang C, Hallett M, Zang Y, Wu X, Chan P. Neuroscience Letters Basal ganglia circuits changes in Parkinson's disease patients. Neurosci Lett. 2012; 524:55–59. https://doi.org/10.1016/j.neulet.2012.07.012. [PubMed: 22813979]

Yanagisawa T, Yamashita O, Hirata M, Kishima H, Saitoh Y, Goto T, Yoshimine T, Kamitani Y. Regulation of Motor Representation by Phase-Amplitude Coupling in the Sensorimotor Cortex. J Neurosci. 2012; 32:15467–15475. https://doi.org/10.1523/JNEUROSCI.2929-12.2012. [PubMed: 23115184]

Yu Q, Erhardt EB, Sui J, Du Y, He H, Hjelm D, Cetin MS, Rachakonda S, Miller RL, Pearlson G, Calhoun VD. Assessing dynamic brain graphs of time-varying connectivity in fMRI data: Application to healthy controls and patients with schizophrenia. Neuroimage. 2015; 107:345–355. https://doi.org/10.1016/j.neuroimage.2014.12.020. [PubMed: 25514514]

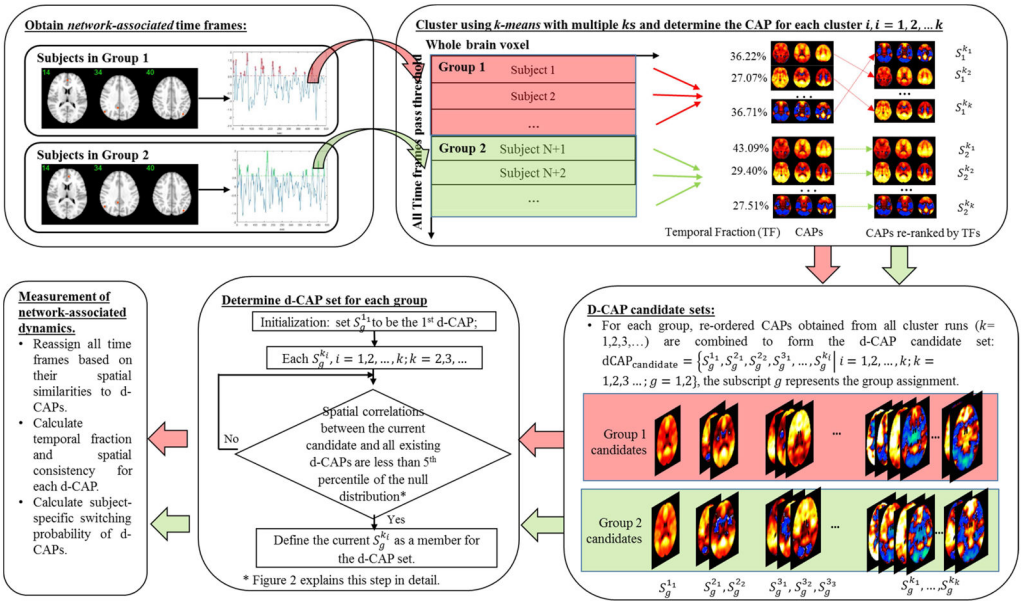

Figure 1.
Group CAP analysis routine.

1. Initialization.
   a. Set $S_g^{1_1}$ in one group to be d-CAP^1 (subscript g represents group assignment);
   b. Number of d-CAPs = 1;
2. For $k = 2,3,\ldots,K$;
   a. For $i = 1,2,\ldots,k$;
      I. Current d-CAP candidate is $S_g^{k_i}$ (superscript k_i denotes the i^{th} cluster of total k clusters);
      II. For $j = 1,2,\ldots,$ number of d-CAPs
         1) Spatial similarity $r_{jk_i} = corr(\text{d-CAP}^j, S_g^{k_i})$;
         2) Determine threshold $thre_{jk_i}$ from null distribution;
            a) For $iter = 1,2,\ldots,200$
               i. Convert the spatial map $S_g^{k_i}$ into vector $S_{g_{vec}}^{k_i}$;
               ii. Randomly permute $S_{g_{vec}}^{k_i}$, obtain $\tilde{S}_{g_{vec}}^{k_i}$;
               iii. Convert $\tilde{S}_{g_{vec}}^{k_i}$ back into spatial map and smooth it with 8mm 3D Gaussian filter (the same smoothness as in d-CAP^j), obtain $\tilde{S}_g^{k_i}$;
               iv. Calculate $r_{jk_{i_{\text{rd}}}}(iter,1) = corr(\text{d-CAP}^j, \tilde{S}_g^{k_i})$;
            b) End for $iter$ loop;
            c) Obtain distribution of $r_{jk_{i_{\text{rd}}}}$: dist$(r_{jk_{i_{\text{rd}}}})$;
            d) Set $thre_{jk_i}$ to be the 5% of the left tail of dist $\left(r_{jk_{i_{\text{rd}}}}\right)$;
            e) If $r_{jk_i} > thre_{jk_i}$ && r_{jk_i}>0.001 && abs(r_{jk_i}-$thre_{jk_i}$)>0.001
               Break; Go to next cluster i;
               End If;
      III. End for j loop;
      IV. Define $S_g^{k_i}$ as a member of the d-CAP set;
      V. Number of d-CAPs = Number of d-CAPs + 1;
   b. End for i loop;
3. End for k loop;

Figure 2.

Algorithm for determining the final d-CAP set. This process is repeated for two groups (g = 1,2) separately and a final d-CAP set is computed for each group individually.

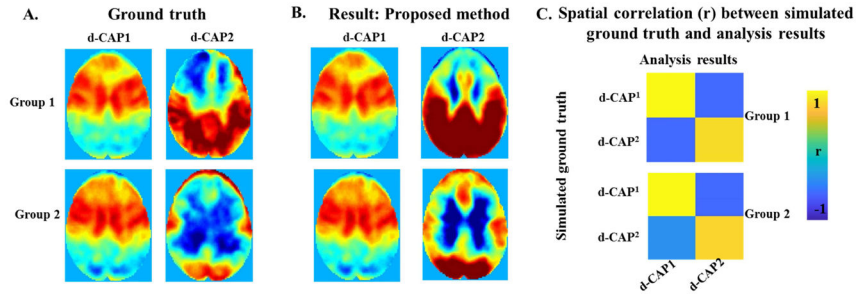

Figure 3-1

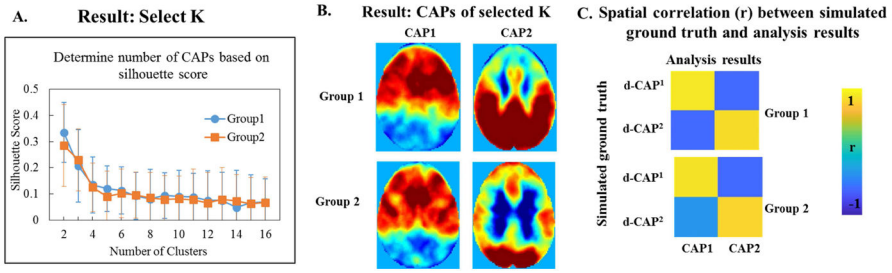

Figure 3-2

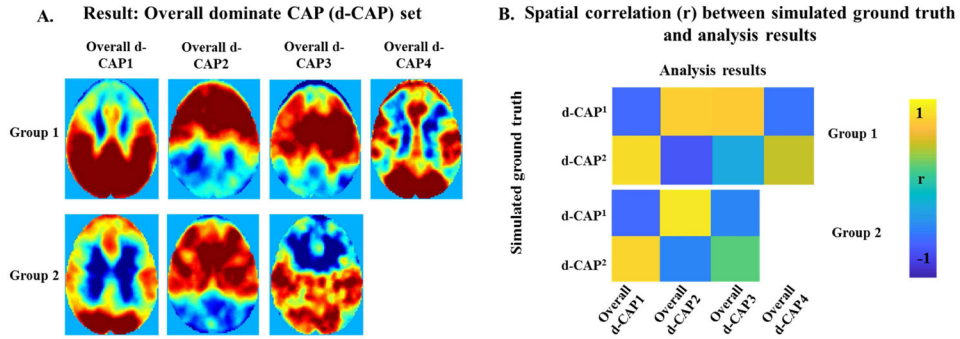

Figure 3-3

Figure 3. Simulation with two d-CAPs

Figure 3-1. Simulation with two d-CAPs in each group. (A). Spatial patterns (average BOLD signal) of simulated d-CAPs (ground-truth slice) in two groups. (B). Spatial patterns (average signal) of d-CAP set computed from the proposed CAP group analysis. (C). Spatial similarities (spatial correlation coefficient) between simulated ground truth and analysis results.

Figure 3-2. CAP set at selected *k* for simulation with two d-CAPs (Chen et al., 2015; Liu and Duyn, 2013). (A). Silhouette scores as a function of cluster numbers. Number of clusters is selected at the highest silhouette score, which gives $k = 2$. (B). Spatial patterns of corresponding two CAPs. (C). Spatial similarities between simulated ground truth and analysis results.

Figure 3-3. Overall d-CAP set (Chen et al., 2015) for simulation with two d-CAPs. (A). Spatial patterns of overall d-CAP set of each group. (B). Spatial similarities between simulated ground truth and analysis results.

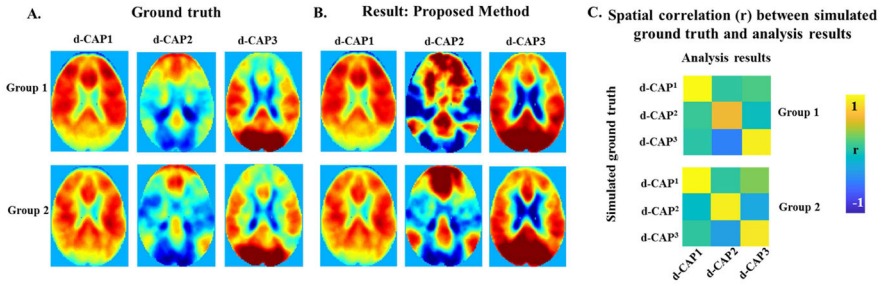

Figure 4-1

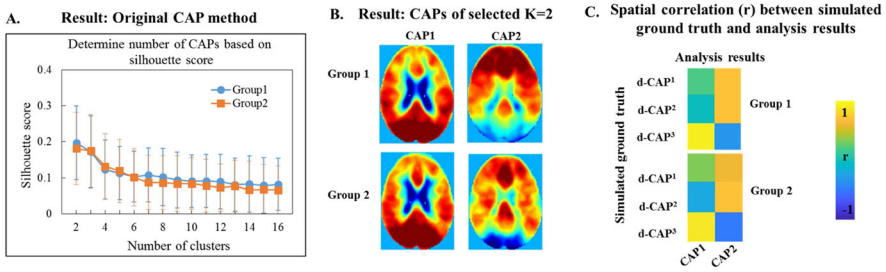

Figure 4-2

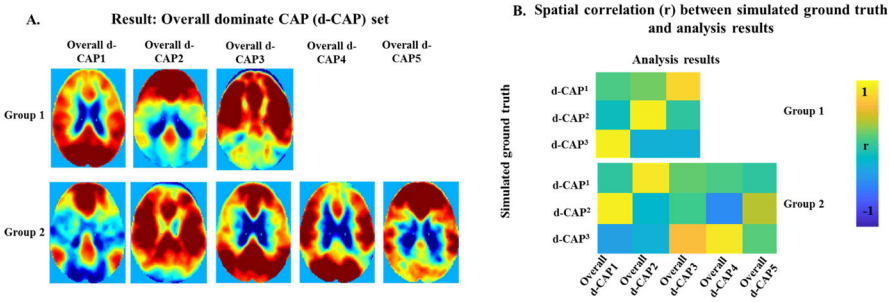

Figure 4-3

Figure 4. Simulation with three d-CAPs

Figure 4-1. Simulation with three d-CAPs in each group. (A). Spatial patterns (average BOLD signal) of simulated d-CAPs (ground-truth slice) in two groups. (B). Spatial patterns (average signal) of d-CAP set computed from CAP group analysis. (C). Spatial similarities (spatial correlation coefficient) between simulated ground truth and analysis results.

Figure 4-2. CAP set at selected k for simulation with three d-CAPs (Chen et al., 2015; Liu and Duyn, 2013). (A). Silhouette scores as a function of cluster numbers. Number of clusters is selected at the highest silhouette score, which gives $k = 2$. (B). Spatial patterns of corresponding two CAPs. (C). Spatial similarities between simulated ground truth and analysis results.

Figure 4-3. Overall d-CAP set for simulation with three d-CAPs (Chen et al., 2015). (A). Spatial patterns of overall d-CAP set of each group. (B). Spatial similarities between simulated ground truth and analysis results.

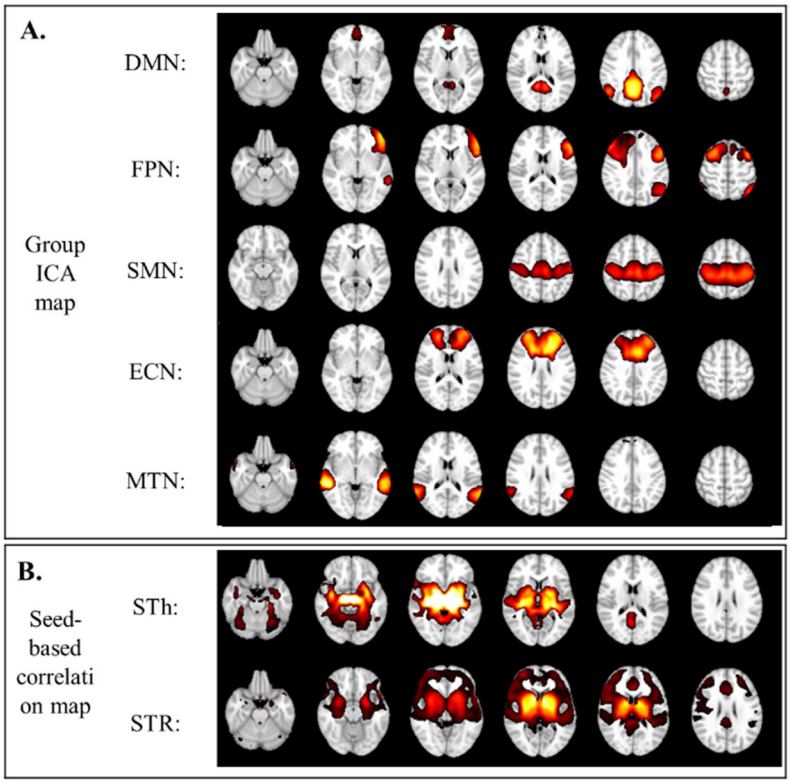

Figure 5.

Spatial maps of seven major networks focused in CAP group analysis: (A) Five ICA component spatial maps and (B) two seed-based correlation maps. Network spatial maps are converted to z-score maps, thresholded at |z|>2 and overlaid on MNI-152 template. Abbreviations: DMN: default mode network; FPN: frontal-parietal network; SMN: sensori-motor network; ECN: executive-control network; MTN: medial temporal network; STh: sub-thalamic seeded network; STR: striatum seeded network.

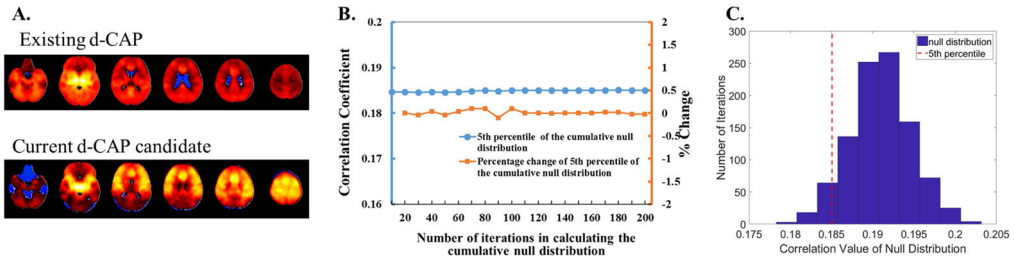

Figure 6-1

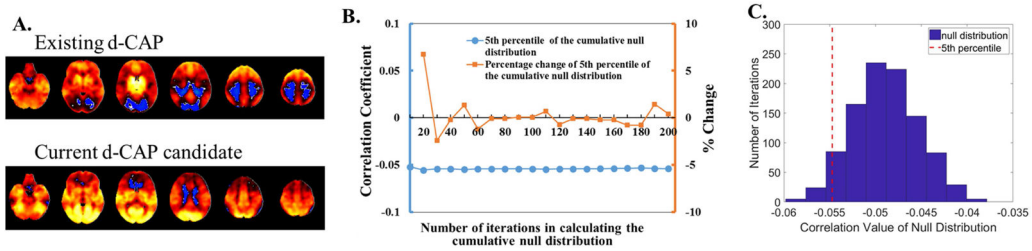

Figure 6-2

Figure 6.

Examples of null distribution of spatial similarity between two maps.

Figure 6-1. (A) Spatial map of the existing d-CAP (top) and the d-CAP candidate (bottom) with a positive spatial correlation (0.09). (B). Statistical threshold (*thre*) in determining the spatial similarity between the two maps as a function of number of permutations being performed. Both *thre* (blue) and the variation (percent change) of *thre* (orange) are plotted against the number of permutations. (C). Null distribution of the spatial correlation value between two maps (blue) and the computed *thre* (dashed red) with 1000 permutations.

Figure 6-2. (A) Spatial map of an existing d-CAP (top) and a d-CAP candidate (bottom) with a negative spatial correlation (-0.21). (B). Statistical threshold (*thre*) in determining the spatial similarity between the two maps as a function of number of permutations being performed. Both *thre* (blue) and the variation (percent change) of *thre* (orange) are plotted against the number of permutations. (C). Null distribution of the spatial correlation value between two maps (blue) and the computed *thre* (dashed red) with 1000 permutations.

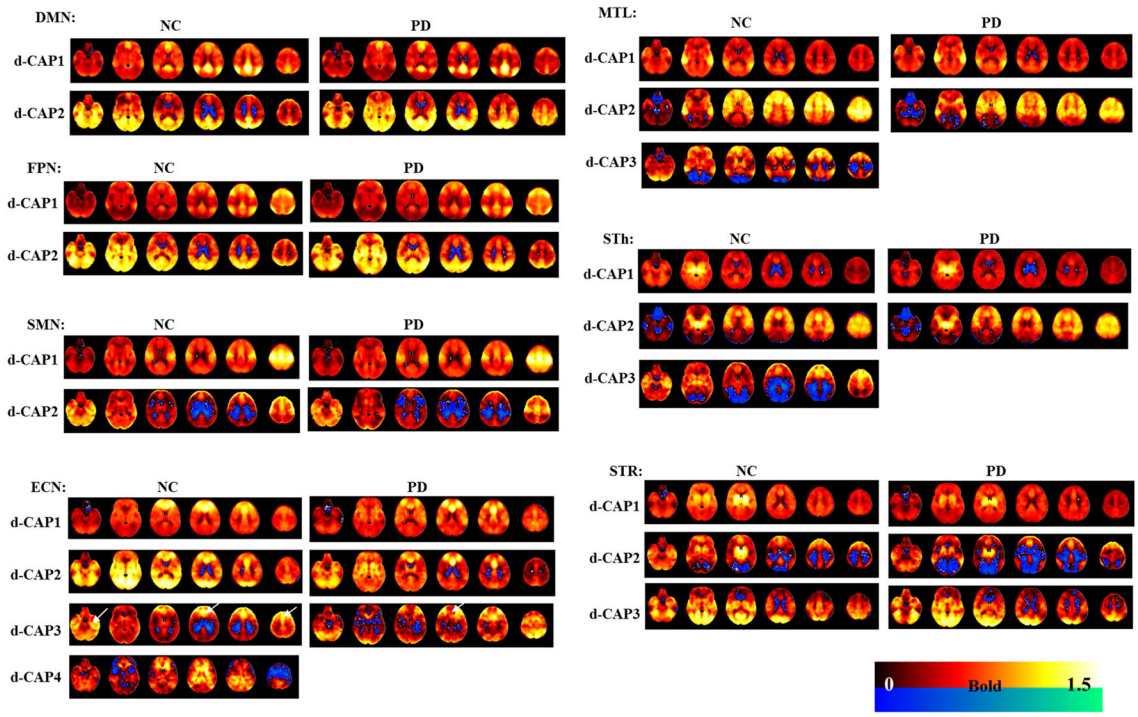

Figure 7-1

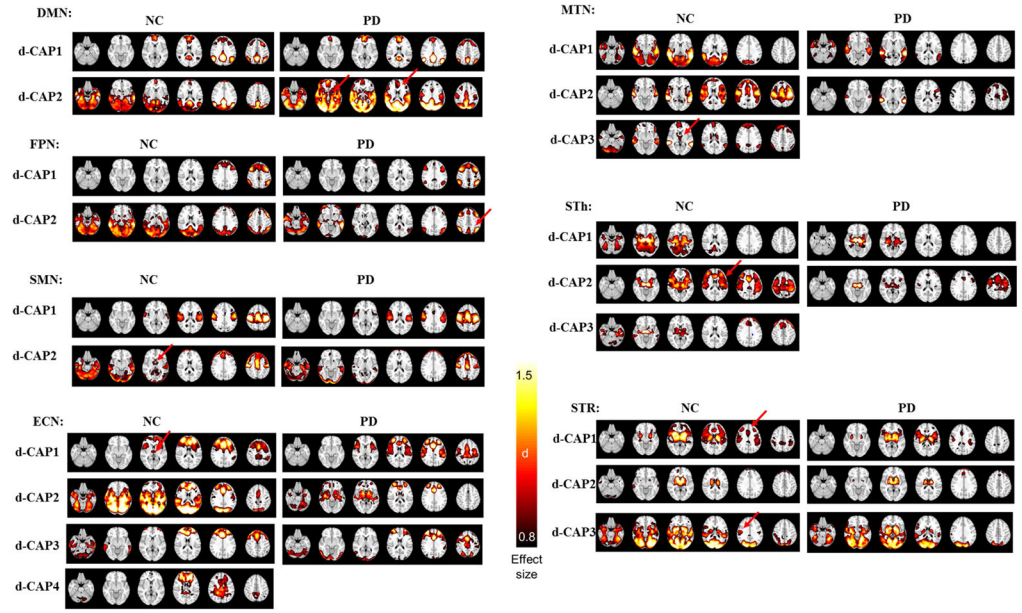

Figure 7-2

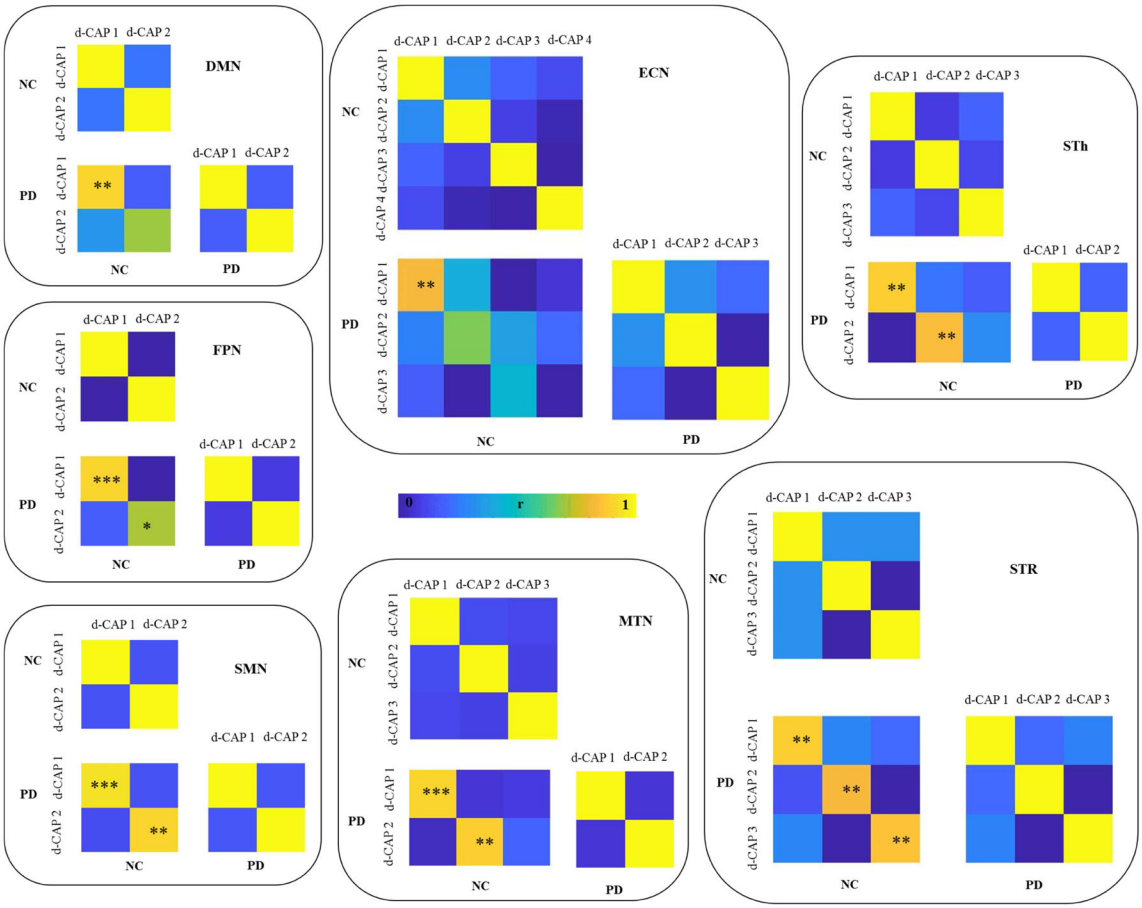

Figure 7-3

Figure 7. D-CAP set in the Parkinson's disease (PD) and normal control (NC) group for different resting-state networks

Figure 7-1. Spatial patterns of d-CAP sets in Parkinson's disease (PD) and normal control (NC) group for different resting-state networks.

Figure 7-2. Effect size (Cohen's d) map of every d-CAP in each group. Maps are thresholded at d>0.8. Red arrows indicate increased co-activations (larger effect size) in one group as compared to the other.

Figure 7-3. Spatial correlation matrices between d-CAPs from the same NC (top left plot in each box) and PD (bottom right plot in each box) group. Spatial correlation matrices d-CAPs from NC and PD groups (bottom right plot in each box). * indicates spatial similarity r>0.7; ** indicates r>0.8 and *** indicates r>0.9.

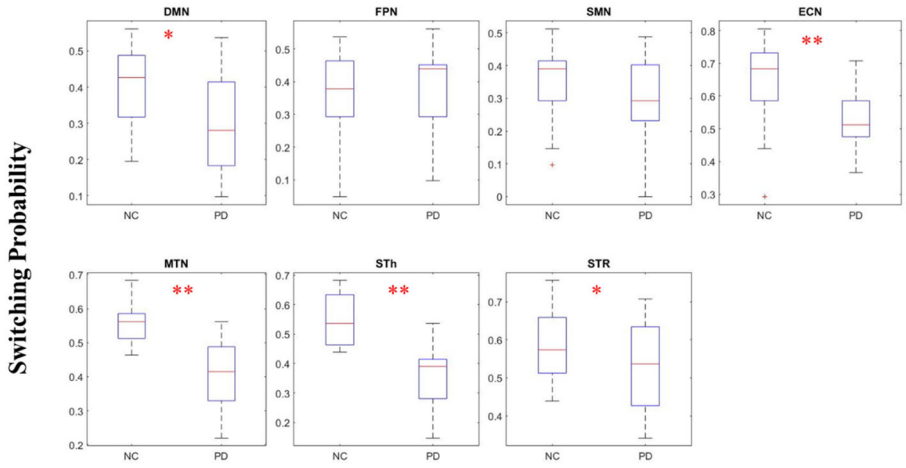

Figure 8.

Box plot of switching probabilities of d-CAPs associated with seven networks in the PD and NC groups. Upper and lower bound of the box represents 75% and 25% of the data, and + indicates outliers. A t-test was performed with age and gender as covariates to test differences in the switching probability of each network for PD and NC groups. * indicates $p<0.05$ (uncorrected) and ** indicates $p<0.05$ (Bonferroni corrected).

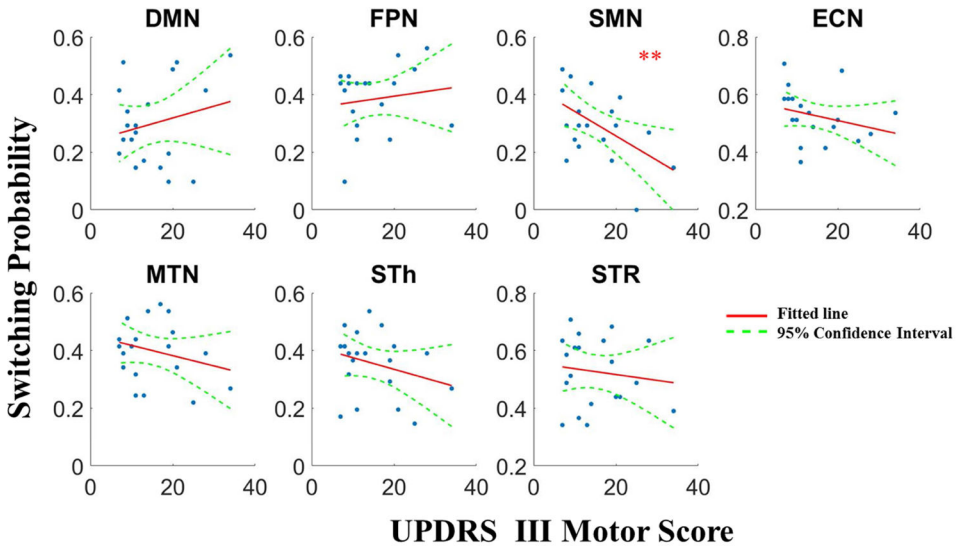

Figure 9.

Switching probability as a function of the UPDRS part-III motor score of PD subjects for different resting-state networks. Age and gender were treated as covariates in the analysis. ** indicates $p<0.05$ after correction for seven comparisons.

Table 1

Demographics of subject cohort. N/A: Not available; RMS: root mean square.

	NC	PD	Statistical
Age	64.25±9.50 (years)	58.03±11.54 (years)	p = 0.10
Gender	14M/4F	11M/9F	p = 0.13
Years of education	16.72±2.67 (years)	16.95±2.86 (years)	p = 0.78
PD disease duration	N/A	1.01±1.07 (years)	N/A
UPDRS III motor score	0.44±1.01	15.05±7.43	p<0.001
UPDRS III tremor score	N/A	1.25±1.04	N/A
RMS Motion	0.58±0.72 (mm)	0.43±0.21 (mm)	p = 0.38

Table 2

Seed locations and corresponding MNI coordinates of seven networks focused in CAP group analysis.

		NC		PD	
	Network	**Region Name**	**Seed Locations**	**Region Name**	**Seed Locations**
Seeds computed from independent components	DMN	R.PCC	4,−50,34	R.PCC	4,−46,34
		R Angular Gyrus	50,−64,36	R Angular Gyrus	50,−60,34
		L Angular Gyrus	−42,−72,40	L Angular Gyrus	−42,−74,38
	FPN	L ACC	−2,46,14	L ACC	−8,44,14
		L Middle Frontal Gyrus	−44,14,48	L Middle Frontal Gyrus	−44,10,50
		L Inferior Parietal Lobule	−50,−56,46	L Inferior Parietal Lobule	−44,−58,48
		R Middle Frontal Gyrus	46,18,46	R Middle Frontal Gyrus	38,12,46
		R Inferior Parietal Lobule	52,−50,54	R Inferior Parietal Lobule	52,−52,52
	SMN	L Precentral Gyrus	−32,−22,48	L Precentral Gyrus	−32, −22, 50
		L Postcentral Gyrus	−34,−24,48	L Postcentral Gyrus	−32, −38, 50
		R Postcentral Gyrus	32, −28, 52	R Postcentral Gyrus	32, −36, 52
		R Precentral Gyrus	32, −20, 52	R Precentral Gyrus	34, −24, 52
	ECN	L Middle Frontal Gyrus	−32,52,20	L Middle Frontal Gyrus	−28,40,28
		R superior Frontal Gyrus	22,44,20	R superior Frontal Gyrus	26,46,24
		L ACC	−10,36,20	L ACC	−6,16,30
	MTN	R Middle Temporal Gyrus	58, −38, 0	R Middle Temporal Gyrus	62, −36, 0
		L Middle Temporal Gyrus	−62, −52, 6	L Middle Temporal Gyrus	−62, −40, 2
Seeds obtained from anatomical atlas	STh	sub-thalamus L	−10,−14,−6	sub-thalamus L	−10,−14,−6
		sub-thalamus R	12,−14,−6	sub-thalamus R	12,−14,−6
	STR	R Putamen	28,−8,6	R Putamen	28,−8,6
		L Putamen	−26,−10,8	L Putamen	−26,−10,8
		R Caudate Nucleus	10,8,12	R Caudate Nucleus	10,8,12
		L Caudate Nucleus	−10,4,12	L Caudate Nucleus	−10,4,12

Abbreviations: DMN: default mode network; FPN: frontal-parietal network; SMN: sensori-motor network; ECN: executive-control network; MTN: medial temporal network; STh: sub-thalamic seeded network; STR: striatum seeded network; L: left; R: right; ACC: anterior cingulate cortex; PCC: posterior cingulate cortex.

Table 3

Number of d-CAPs in PD and NC groups for resting-state networks used in the CAP group analysis.

Network	NC	PD
DMN	2	2
FPN	2	2
SMN	2	2
ECN	4	3
MTN	3	2
STh	3	2
STR	3	3

Table 4

Between group differences in the thresholded effect size map (Cohen's d>0.8) of each d-CAP. (A) Increased activities in NC group. (B) Increased activities in the PD group.

A.

	Network	d-CAPs	Increased activities (larger effect size) in the NC group
Network with the same number of d-CAPs	SMN	2nd d-CAP	Sub-cortical areas
	STR	3rd d-CAP	Motor areas
	STR	1st d-CAP	Frontal areas
Networks with one more d-CAPs in the NC group	MTN	2nd d-CAP	Frontal areas
	STh	2nd d-CAP	Motor areas
	ECN	2nd d-CAP	Sub-cortical areas
	STh		Frontal areas
	MTN	The additional d-CAPs in NC	Sub-cortical areas
	ECN		Anterior cingulate cortex

B.

	Network	d-CAPs	Increased activities (larger effect size) in the PD group
Network with the same number of d-CAPs	DMN	2nd d-CAP	Superior temporal lobe, middle frontal areas
	FPN	3rd d-CAP	Inferior parietal lobe

Table 5

(A) Temporal fraction of each d-CAP associated with seven networks in PD and NC groups. (B) Statistical comparisons of the temporal fraction of the 1st d-CAP associated with networks that share the same number of d-CAPs in the PD and NC groups. Mean and standard deviation (std) of subject temporal fractions are shown in the first two rows. Network-specific t-values, family-wise corrected p-values (Bonferroni corrected) and effect size (Cohen's d) of the temporal fraction of the 1st d-CAPs for the contrast NC > PD.

A.

	NC				PD		
	d-CAP1	**d-CAP2**	**d-CAP3**	**d-CAP4**	**d-CAP1**	**d-CAP2**	**d-CAP3**
DMN	67.21%	32.79%			75.85%	24.15%	
FPN	74.66%	25.34%			72.93%	27.07%	
SMN	75.07%	24.93%			78.54%	21.46%	
ECN	48.24%	22.09%	19.51%	10.16%	55.98%	28.41%	15.61%
MTN	55.56%	24.39%	20.05%		68.17%	31.83%	
STh	56.91%	26.29%	16.80%		69.88%	30.12%	
STR	50.54%	27.37%	22.09%		54.63%	22.56%	22.80%

B.

Network	**Mean and std of the temporal fraction**		**T-value**	**Family-wise corrected p-value**	**Effect size**
	NC	**PD**			
DMN	67.21%±10.06%	75.85%±15.94%	−1.58	0.50	0.58
FPN	74.66%±11.24%	72.93%±10.57%	0.25	1.00	0.09
SMN	75.07%±14.05%	78.54%±9.65%	−1.56	0.52	0.57
STR	50.54%±11.86%	54.63%±13.03%	−1.34	0.76	0.49

Table 6

Spatial consistency and the 95th percentile of its null distribution (in parenthesis) of each d-CAP associated with seven networks for the PD and NC groups.

	NC				PD		
	d-CAP1	**d-CAP2**	**d-CAP3**	**d-CAP4**	**d-CAP1**	**d-CAP2**	**d-CAP3**
DMN	0.29 (0.21)	0.32 (0.22)			0.28 (0.23)	0.30 (0.24)	
FPN	0.28 (0.21)	0.32 (0.23)			0.30 (0.23)	0.28 (0.24)	
SMN	0.35 (0.28)	0.34 (0.30)			0.32 (0.27)	0.31 (0.29)	
ECN	0.36 (0.22)	0.35 (0.23)	0.36 (0.24)	0.34 (0.25)	0.33 (0.21)	0.30 (0.22)	0.29 (0.24)
MTN	0.32 (0.21)	0.37 (0.23)	0.34 (0.23)		0.26 (0.18)	0.28 (0.19)	
STh	0.35 (0.23)	0.35 (0.25)	0.38 (0.25)		0.27 (0.20)	0.31 (0.22)	
STR	0.32 (0.21)	0.32 (0.22)	0.36 (0.23)		0.29 (0.20)	0.32 (0.21)	0.35 (0.21)

Table 7

Statistical comparisons of switching probability in the NC and PD groups. Mean and standard deviation (std) of switching probability in each network are listed separately for two groups. Network-specific t-values, family-wise corrected p-values (Bonferroni corrected) and effect size (Cohen's d) of the switching probability for the contrast NC > PD are also listed.

Network	Mean and std of the switching probability		T-value	Family-wise corrected p-value	Effect size
	NC	PD			
DMN	0.40 ± 0.11	0.30 ± 0.14	2.20	0.25	0.79
FPN	0.36 ± 0.13	0.38 ± 0.11	0.14	1.00	0.05
SMN	0.35 ± 0.12	0.30 ± 0.12	1.73	0.65	0.62
ECN	0.64 ± 0.12	0.53 ± 0.09	2.89	0.05	1.04
MTN	0.56 ± 0.06	0.40 ± 0.10	4.91	1.9×10^{-4}	1.77
STh	0.55 ± 0.08	0.35 ± 0.11	5.59	2.7×10^{-5}	2.01
STR	0.59 ± 0.09	0.53 ± 0.12	2.47	0.13	0.89

Table 8

Network-specific t-values, family-wise corrected p-values (Bonferroni corrected) and effect size (Cohen's d) for the switching probability as a linear function of the UPDRS-III motor score in PD.

Network	T-value	Family-wise corrected p-value	Effect size
DMN	0.58	1.00	0.16
FPN	0.84	1.00	0.22
SMN	−3.31	0.04	0.88
ECN	−0.95	1.00	0.25
MTN	−0.81	1.00	0.22
STh	−0.85	1.00	0.23
STR	0.66	1.00	0.18